DIFFUSION OF MAGNETIC AND ELECTRIC FIELDS INTO A CONDUCTING MEDIUM

by

Michael Stock

Submitted in Partial Fulfillment

of the Requirements for the Degree of

Master of Science in Physics

New Mexico Institute of Mining and Technology

Socorro, New Mexico

August, 2010

ABSTRACT

The earth is an imperfect conductor with a resistivity on the order of 100 $\Omega \cdot$ m. Therefore the azimuthal magnetic field produced by a lightning return stroke will diffuse into the ground. Frequency components of the magnetic field below about 10 kHz will be significant and measurable more than 100 m below the surface. A radial electric field is also present in the ground which can be calculated from the vertical gradient of the magnetic field. The ground acts like a band-pass filter on the electric field, with a response peaking between 1 and 10 kHz. On January 2, 2006, there was a methane air explosion in a sealed area of the Sago mine in West Virginia. The explosion was associated with a +101 kA lightning return stroke to ground which occurred within two miles of the explosion origin. While there was no direct conducting path from the surface into the sealed area of the mine, at the epicenter of the explosion was one end of a 400 m pump cable lying along the floor of the mine. The electric field in the ground can produce a potential difference between the ground and the pump cable. To calculate the magnitude of the this potential difference, first a lightning strike was modeled as the radiation produced by a finite length transmission line excited by a triangular current pulse. Then the electric and magnetic fields at the depth of the mine were calculated by applying the diffusion equations to the surface fields. Finally the potential difference on the pump cable is found by integrating the electric field along the cable. For the lightning strike associated with the Sago mine explosion, the peak voltage on the pump cable is estimated to be 1150 V.

CONTENTS

This report is accepted on behalf of the faculty of the Institute by the following committee:

Paul Krehbiel, Advisor

I release this document to the New Mexico Institute of Mining and Technology.

Michael Stock Date

CHAPTER 1

INTRODUCTION

On January 2, 2006 a methane air explosion in a sealed area of the Sago mine in West Virginia resulted in the death of 12 miners. The explosion was determined to have occurred at 6:26 a.m. 35 seconds; at 6:26 a.m. 35.680 seconds there was a +101 kA lightning ground stroke within two miles of the origin of the explosion (see Figure 1.0.1) [Wooten, 2006]. This sharp correlation strongly implies that the lightning strike was the cause of the explosion, however there were no direct conduction paths into the sealed area of the mine.

The Sago mine was active at the time of the explosion and still producing coal. The explosion occurred in a sealed area of the mine, two miles from the mine head and 100m below the local surface. The area was physically as well as electrically isolated from the rest of the mine by a seal made of special seal blocks. Because the area was physically separated from the active areas of the mine, it could not be ventilated, causing a buildup of methane gas inside the sealed area which was highly explosive at the time of the lightning strike. A buildup of methane gas in a sealed areas of mines is normal. As the concentration of methane increases it passes through an explosive phase; once the concentration is high enough, the sealed area will no longer be explosive. The only suspicious component inside the sealed area of the mine was a 400m long pump cable, one end of which was at the epicenter of the explosion. This pump cable was entirely contained inside the sealed area of the mine.

An initial investigation into the possibility of lightning initiating a spark inside the sealed area of the mine was made by Sandia National Laboratory in 2006 [Higgins & Morris, 2006]. This investigation centered on whether a lightning strike could cause a large enough

potential along the pump cable to cause a spark. The authors of the Sandia study investigated two methods by which a lightning strike could have cause a spark: a direct coupling method and an indirect coupling method. In the direct coupling method, current from the lightning strike travels down the rail car tracks or power cables in the active area of the mine and jumps across the seal. In the indirect coupling method, fields from a lightning strike above ground penetrate the ground into the mine through diffusion and induce a voltage on the pump cable. The authors determined that the direct coupling method could not have produced a spark inside the sealed area of the mine, but the indirect coupling method possibly could. For the indirect coupling method to produce large enough potentials in the mine, a horizontal current channel approximately 100m above the ground, as opposed to a vertical current channel as seen in a cloud-to-ground lightning flash, had to be used as the input. Horizontal current channels commonly occur in thunderstorms, but low altitude high-current channels parallel to the ground do not [Krehbiel et al., 1979, Thomas et al., 2004].

A followup investigation was made by New Mexico Tech in 2007 and 2008 where direct measurements of the electric and magnetic fields inside the mine were made, as well as the voltages produced on the pump cable. The 2007 measurements showed voltage waveforms produced by cloud-to-ground lightning strokes having amplitudes of hundreds to thousands of volts. The measurements were highly time correlated with lightning strikes, however they lacked the azimuthal dependence expected if a diffusion process was coupling the lightning strike to the mine. The 2008 measurements showed voltage waveforms having smaller peak amplitudes of less than 150V. In addition the azimuthal dependence expected from diffusion was present.

This paper is an extension of the work started in the Sandia report. A method of calculating the voltage seen on the pump cable produced by a cloud-to-ground lightning strike is developed. This is done in a three step process – first the fields above the mine at the surface

are obtained, then a set of diffusion equations act on the surface fields to produce the fields in the ground, and finally the voltage on the pump cable can be calculated knowing the fields in the ground. This paper concentrates on the theoretical background to diffusing fields produced by lightning strikes into the ground. Comparisons of the theoretical results to measurements made in 2007 and 2008 will be done separately.

In Section 2.1, the differential form of the diffusion equations are derived from first principles. The differential equations are solved in Cartesian coordinates in Section 2.3 and cylindrical coordinates in Section 2.4. The numerical implementation of solving the diffusion equations is done using FFTs; this allows arbitrary fields to be used as the input for the diffusion equations. Details of the FFT implementation are presented in Appendix A. To obtain input for the diffusion equations, models for the fields of a lightning strike are developed in Section 3. These models start with a magnetostatic approximation in Section 3.1 and continue to more complex electrodynamic models in Section 3.2. Finally, the results of the lightning models are used as the input for the diffusion equations in Section 4 to calculate the fields in the ground. Once the fields in the ground are known, some simple calculations are made to estimate the voltage on the pump cable in Section 4.3.

1.1 Prior Work

Some prior work has been done in this regard. For blasting operations in underground mines in the Alps, K. Berger [Golde, 1977] found that currents in the ground produced by lightning were sufficient to cause premature detonation of the explosives. He described a mine as a conducting shaft embedded in a highly resistive medium. Mine shafts and tunnels conduct because of metal pipes, power lines and rail car track that are laid in it. Because solid rock is highly resistive, a current flowing through it can cause large potential differences. Berger was

particularly interested in the currents flowing through the face of the mine, where the detonators are placed when constructing a mine shaft. He conducted lab measurements to determine what these currents should be, and the design of the detonators was modified accordingly. In these studies, Berger was studying stone such as granite with very high resistivities between 3,000 and 10,000 $\Omega \cdot$ m. The rock above the Sago mine consists of many layers of different compositions having resistivity values typically of a few hundred $\Omega \cdot$ m. The lower resistivities cause the fields produced by a lightning strike to not penetrate as deeply into the ground.

Park and Dejnakarintra looked at the penetration of electric fields into the ionosphere first for DC fields [Park & Dejnakarintra, 1973] and then for time-varying fields [Dejnakarintra & Park, 1974]. At first, it may appear that penetration of fields into the ionosphere would bear little resemblance to penetration of fields into the ground. However, the same diffusion equations apply; the conductivities in the ionosphere and the ground are different, but the underlying physics is the same. To solve the problem in the ionosphere, Park and Dejnakarintra assumed an exponential conductivity profile with altitude, $\sigma = a \exp(\beta z)$, which is a good approximation of the conductivity in the atmosphere. An exponential profile allows the $\nabla\sigma$ terms of the diffusion equations to be treated analytically. For the ground, an exponential conductivity profile is not appropriate, so the same analytic methods can not be used.

The work done by Delfino and Rachid [Delfino & Rachid, 2007] is perhaps the most applicable to this problem. They used a model of a lightning strike as an antenna excited by a current pulse traveling up the lightning channel like a transmission line, similar to a model developed by Uman et al. [Uman et al., 1974] but in the frequency domain. Sommerfeld's solution for a point dipole radiator over a imperfect conductor was adapted for use with a finite length antenna [Sommerfeld, 1949]. The analytic solutions were numerically evaluated to obtain the fields in the earth very close to the lightning channel (the Sommerfeld model breaks down within one wavelength of the radiator [Sommerfeld, 1949]).

The primary disadvantage of the technique developed by Delfino and Rachid is that the model for the fields produced by the lightning channel can not be separated from the calculation of the fields in the ground. This method is limited to using a transmission line model to approximate the fields produced by a lightning flash; it can not be applied to in situ measurements. In addition, the treatment is mathematically complex and it is difficult to obtain a physical understanding of the processes taking place.

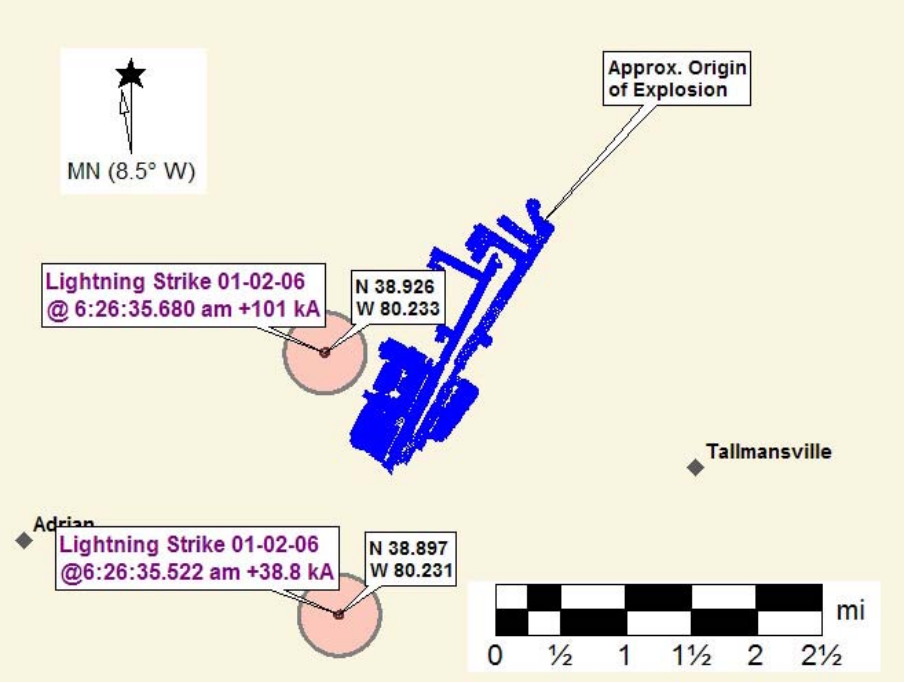

Figure 1.0.1: Lightning Strike located by Vaisala nearby the Sago Mine at the time of the explosion [Wooten, 2006].

CHAPTER 2

THE DIFFUSION EQUATIONS

Consider a vertical channel carrying a current $I(t)$ over an imperfect conductor, as is the case with a cloud to ground lightning strike and depicted in Figure 2.0.1. The geometry is azimuthally symmetric, and will produce a magnetic field $\vec{B}(t)$ in the $\hat{\phi}$ direction and an electric field in the $\hat{z}$ direction. The electric field $\vec{E}(t)$ is restricted to the $\hat{z}$ and $\hat{r}$ directions by the symmetry of the problem. If the conductor is good (ρ_c on the order of 100 $\Omega \cdot$ m), the radial component of the electric field will be dwarfed by the vertical component near the surface. For this reason the radial fields at the surface are generally neglected. The magnitude of these fields at the surface within a few kilometers of the lightning strike are on the order of a kV/m for the vertical electric field and an A/m for the magnetic field[1].

Both the magnetic and electric fields will penetrate into the conductor because the conductivity is finite. In a perfect conductor, there will be a surface current $\vec{K}$ in the $\hat{r}$ direction. In an imperfect conductor, there is a current density $\vec{J}$ in the $\hat{r}$ direction. Conservation of charge implies that the current density is the source for the current $I(t)$ flowing up the lightning channel. Neglecting any gradients in the conductivity, the penetration of all these fields into the ground is governed by the well known diffusion equation:

$$\nabla^2 \vec{F}(t, \vec{x}) = k \frac{\partial}{\partial t} \vec{F}(t, \vec{x}) \tag{2.0.1}$$

[1]Here the magnetic field $\vec{B}(t)$ is associated to units of A/m, which is usually used for the auxiliary field $\vec{H}(t)$. This is done entirely for convenience of the magnitude of the measurement, but may lead to some confusion. However in the absence of large deposits of iron in the conductor, $\mu = \mu_0$ and the units are unambigious.

where k is a constant. What follows is the derivation of equation 2.0.1 from first principals. This derivation is kept as general as possible. At the end, the general equation is simplified for the specific problem described above. This allows any approximations made to be investigated so that their effect is better understood.

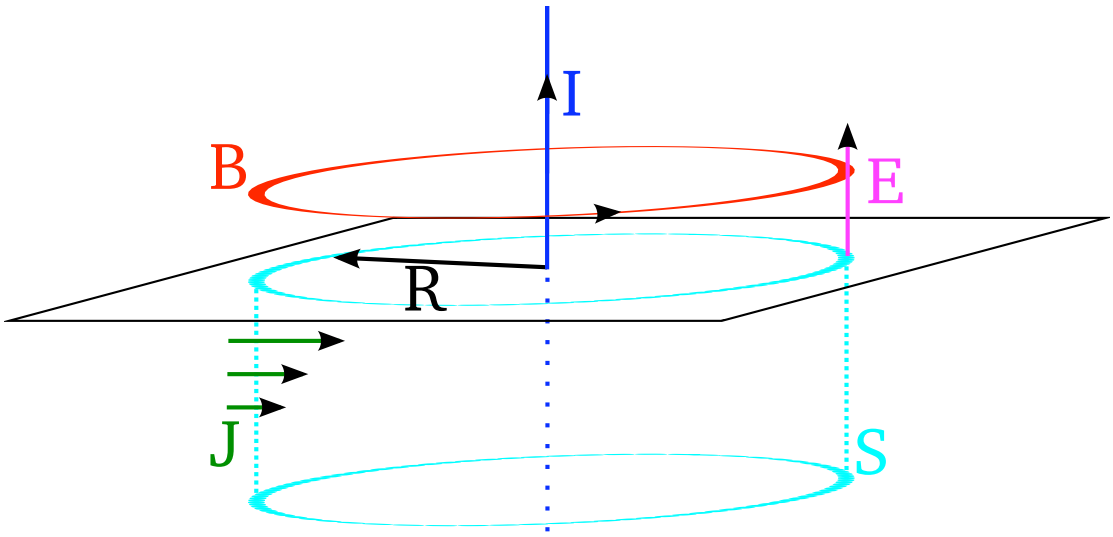

Figure 2.0.1: A vertical current channel over an imperfect conductor. The fields produced by the current channel penetrate into the conductor, reducing in amplitude with depth. The magnetic field induces a radial electric field (or current density) which should be consistent with the vertical current channel above the conductor.

2.1 Derivation of Diffusion Equations

The derivation of the diffusion equations for electric and magnetic fields is presented by Jackson [Jackson, 1999] neglecting the effects of the displacement current and assuming uniform conductivity. However, even if the conductivity of the conductor is perfectly uniform, there is still a non-zero gradient term at the surface. This term is important and should not lightly be neglected. The effect of the displacement current is generally small unless the conductivity is very poor or the frequency is very high, but it is fairly easy to treat and so is included in this derivation.

Starting with Maxwell's equations we have:

$$\begin{aligned}
\nabla \cdot \vec{B} &= 0 \\
\nabla \cdot \vec{E} &= \frac{\rho}{\epsilon_0} \\
\nabla \times \vec{E} &= -\frac{\partial \vec{B}}{\partial t} \\
\nabla \times \vec{B} &= \mu_0 \vec{J} + \mu_0 \epsilon_0 \frac{\partial \vec{E}}{\partial t}
\end{aligned}$$

It is convenient to consider fields in harmonic form, $\vec{F}(t) = \tilde{F} e^{i\omega t}$, where $\tilde{F}$ is a complex amplitude. To obtain the diffusion equations, we will concentrate on Ampére and Faraday's Laws, and introduce Ohm's Law as a necessary approximation to solve for $\tilde{B}$ and $\tilde{E}$. This gives the following,

$$\nabla \cdot \tilde{B} = 0 \tag{2.1.1}$$

$$\nabla \cdot \tilde{E} = \frac{\rho}{\epsilon_0} \tag{2.1.2}$$

$$\nabla \times \tilde{E} = -i\omega \tilde{B} \tag{2.1.3}$$

$$\nabla \times \tilde{B} = \mu_0 \tilde{J} + i\omega \mu_0 \epsilon_0 \tilde{E} \tag{2.1.4}$$

$$\tilde{J} = \sigma \tilde{E} \tag{2.1.5}$$

Ohm's Law can immediately be used to simplify the form of Ampère's Law, which is more appropriate for this problem.

$$\nabla \times \tilde{B} = \mu_0 \left(\sigma + i\omega \epsilon_0\right) \tilde{E} \tag{2.1.6}$$

To arrive at the diffusion equations from Maxwell's equations in harmonic form, the following vector identities will be required

$$\begin{aligned}
\nabla \times \left(\nabla \times \vec{A}\right) &= \nabla \left(\nabla \cdot \vec{A}\right) - \nabla^2 \vec{A} \\
\nabla \times \left(f \vec{A}\right) &= f \left(\nabla \times \vec{A}\right) - A \times \nabla f \\
\nabla \cdot \left(f \vec{A}\right) &= f \nabla \cdot \vec{A} + A \cdot \nabla f
\end{aligned}$$

where f is a scalar and $\vec{A}$ is a vector.

To solve for $\tilde{B}$, take the curl of equation 2.1.6 and apply some vector identities. Then substitute in equation 2.1.3.

$$\begin{aligned} \nabla \times \left(\nabla \times \tilde{B}\right) &= \nabla \times \left(\mu_0 \left(\sigma + i\omega\epsilon_0\right) \tilde{E}\right) \\ \nabla \left(\nabla \cdot \tilde{B}\right) - \nabla^2 \tilde{B} &= \mu_0 \left(\sigma + i\omega\epsilon_0\right) \nabla \times \tilde{E} - \tilde{E} \times \nabla \left(\mu_0 \sigma + i\omega\mu_0\epsilon_0\right) \\ \nabla^2 \tilde{B} &= i\omega\mu_0 \left(\sigma + i\omega\epsilon_0\right) \tilde{B} + \mu_0 \tilde{E} \times \nabla\sigma \end{aligned} \tag{2.1.7}$$

Equation 2.1.7 is coupled to the electric field. To obtain a form dependent only on the magnetic field, notice that:

$$\begin{aligned} \mu_0 \tilde{E} \times \nabla\sigma &= \mu_0 \tilde{E} \times \nabla\sigma \frac{\sigma + i\omega\epsilon_0}{\sigma + i\omega\epsilon_0} \\ &= \frac{\mu_0 \left(\tilde{E}(\sigma + i\omega\epsilon_0)\right) \times \nabla\sigma}{\sigma + i\omega\epsilon_0} \\ &= \frac{\left(\nabla \times \tilde{B}\right) \times \nabla\sigma}{\sigma + i\omega\epsilon_0} \end{aligned} \tag{2.1.8}$$

in which case equation 2.1.7 becomes

$$\nabla^2 \tilde{B} = i\omega\mu_0 \left(\sigma + i\omega\epsilon_0\right) \tilde{B} + \frac{\left(\nabla \times \tilde{B}\right) \times \nabla\sigma}{\sigma + i\omega\epsilon_0} \tag{2.1.9}$$

Solving for $\tilde{E}$ can be done in a similar fashion.

$$\begin{aligned} \nabla \times \left(\nabla \times \tilde{E}\right) &= \nabla \times \left(-i\omega\tilde{B}\right) \\ \nabla \left(\nabla \cdot \tilde{E}\right) - \nabla^2 \tilde{E} &= -i\omega \nabla \times \tilde{B} \\ \nabla^2 \tilde{E} &= i\omega\mu_0 \left(\sigma + i\omega\epsilon_0\right) \tilde{E} + \nabla \left(\nabla \cdot \tilde{E}\right) \end{aligned} \tag{2.1.10}$$

Unlike the case with the magnetic field, the divergence of the electric field is not automatically

zero. This term can be found by taking the divergence of equation 2.1.6.

$$\begin{aligned}
\nabla \cdot \left(\nabla \times \tilde{B}\right) &= \nabla \cdot \left(\mu_0 \left(\sigma + i\omega\epsilon_0\right) \tilde{E}\right) \\
0 &= \mu_0 \left(\sigma + i\omega\epsilon_0\right) \nabla \cdot \tilde{E} + \tilde{E} \cdot \mu_0 \nabla \left(\sigma + i\omega\epsilon_0\right) \\
\left(\sigma + i\omega\epsilon_0\right) \nabla \cdot \tilde{E} &= -\tilde{E} \cdot \nabla\sigma \\
\nabla \cdot \tilde{E} &= -\frac{\tilde{E} \cdot \nabla\sigma}{\left(\sigma + i\omega\epsilon_0\right)}
\end{aligned} \tag{2.1.11}$$

And equation 2.1.10 becomes

$$\nabla^2 \tilde{E} = i\omega\mu_0 \left(\sigma + i\omega\epsilon_0\right) \tilde{E} - \nabla \frac{\tilde{E} \cdot \nabla\sigma}{\left(\sigma + i\omega\epsilon_0\right)} \tag{2.1.12}$$

Equations 2.1.9 and 2.1.12 are the diffusions equations for electric and magnetic fields in a conducting medium. They are fully generic and both have a similar form:

$$\nabla^2 \tilde{F} = i\omega\mu_0 \left(\sigma + i\omega\epsilon_0\right) \tilde{F} + b(\nabla\sigma, \tilde{F}) \tag{2.1.13}$$

where $i\omega\mu_0 \left(\sigma + i\omega\epsilon_0\right) \tilde{F}$ is the diffusion term and $b(\nabla\sigma, \tilde{F})$ is a function of $\nabla\sigma$ which is unique to the specific field. If this term is neglected (in the presence of a uniform conductor for example) then these equations reduce to:

$$\begin{aligned}
\nabla^2 \tilde{F} &= i\omega\mu_0 \left(\sigma + i\omega\epsilon_0\right) \tilde{F} \\
\nabla^2 F &= \mu_0 \tilde{\sigma} \frac{\partial}{\partial t} F
\end{aligned} \tag{2.1.14}$$

where $\tilde{\sigma}$ is the complex conductivity, conductivity including the effects of the displacement current. While the complex conductivity has a small dependence on frequency, equation 2.1.14 is clearly the same as equation 2.0.1 with $k = \mu_0\tilde{\sigma}$. In addition, if there are no spatial gradients of σ or μ, then this holds for the auxiliary field $\tilde{H}$ and the current density $\tilde{J}$ as well.

2.2 Simplification of the General Diffusion Equations

Equations 2.1.9 and 2.1.12 are the fully general diffusion equations for electric and magnetic fields. They are true for any electric or magnetic field in any conductor; as such, they can be applied to a wide variety of different problems. When applying the diffusion equations to the problem under investigation in this study and described in Figure 2.0.1, equations 2.1.9 and 2.1.12 simplify.

2.2.1 Displacement Current

The quantity $\sigma + i\omega\epsilon_0$ is the complex conductivity, where the $i\omega\epsilon_0$ term comes from the displacement current. It should therefore include the effects of time delay from the finite speed of propagation of the fields. This effect can be safely neglected if $\omega \ll \sigma/\epsilon_0$. For earth, $\sigma \sim 1/100\ \Omega^{-1}\text{m}^{-1}$, so the displacement current can be neglected for $\omega \ll 1^9$ rad/s, or for frequencies less than about 150 MHz. Since the mine is about 100 m beneath the surface, the ground acts as a fairly strong low-pass filter and frequencies above about 60 kHz can be neglected (see Figure 2.3.2). This means that equations 2.1.9 and 2.1.12 can be simplified to

$$\nabla^2\tilde{B} = i\omega\mu_0\sigma\tilde{B} + \frac{(\nabla\times\tilde{B})\times\nabla\sigma}{\sigma} \tag{2.2.1}$$

$$\nabla^2\tilde{E} = i\omega\mu_0\sigma\tilde{E} - \nabla\frac{\tilde{E}\cdot\nabla\sigma}{\sigma} \tag{2.2.2}$$

2.2.2 Vertical Gradients

In the case of a layered conductor (including a conductor with only a single layer), the last term in equations 2.2.1 and 2.2.2 can be simplified somewhat because $\nabla\sigma$ only has a com-

ponent in the $\hat{z}$ direction:

$$\nabla^2 \tilde{B}_\phi = i\omega\mu_0\sigma\tilde{B}_\phi - \frac{1}{\sigma}\frac{\partial\sigma}{\partial z}\frac{\partial\tilde{B}_\phi}{\partial z} \tag{2.2.3}$$

$$\nabla^2 \tilde{E}_z = i\omega\mu_0\sigma\tilde{E}_z - \nabla\left(\frac{\tilde{E}_z}{\sigma}\frac{\partial\sigma}{\partial z}\right) \tag{2.2.4}$$

$$\nabla^2 \tilde{E}_r = i\omega\mu_0\sigma\tilde{E}_r \tag{2.2.5}$$

2.2.3 Boundary Terms

Equation 2.1.13 has an additional term, $b(\nabla\sigma, \tilde{F})$, which is not present in the classical diffusion equation 2.0.1 and adds complexity. Figure 2.0.1 has only a single slab of conductivity, so $\nabla\sigma$ can be reduced to $d\sigma/dz\ \hat{z}$. In addition, because the conductor is uniform, the only place where $d\sigma/dz \neq 0$ is at the air-earth boundary. In a more complex model with a number of horizontally stratified layers of uniform conductivity, $d\sigma/dz \neq 0$ at each of the boundary of each layer. So, the $\nabla\sigma$ term can be thought of as a boundary term.

The effects of this boundary term are not obvious just by looking at equations 2.1.9 and 2.1.12. In addition, implementing this term in a numerical model, such as the one presented here, is non-trivial. Traditionally, the boundary terms are neglected, however, first it must be understood.

In the general diffusion equation for the magnetic field, equation 2.1.9, the boundary term is given by:

$$b(\nabla\sigma, \tilde{F}) = \frac{(\nabla\times\tilde{B})\times\nabla\sigma}{\sigma + i\omega\epsilon_0} \tag{2.2.6}$$

Because the conductivity is uniform above and below the air-earth boundary ($z = 0$), $\nabla\sigma = -\sigma\delta(z)\hat{z}$, where $\delta(z)$ is a Dirac delta function. $\tilde{B}$ is entirely in the $\hat{\phi}$ direction so using equations 2.1.4 and 2.1.5, $\nabla\times\tilde{B} = -\mu_0(\sigma + i\omega\epsilon_0)\tilde{J}/\sigma\ \hat{r}$. In this case, the last term of equation 2.1.9

becomes:

$$\begin{aligned}\frac{(\nabla \times \tilde{B}) \times \nabla\sigma}{\sigma + i\omega\epsilon_0} &= \frac{(\mu_0(\sigma + i\omega\epsilon_0)/\sigma)\tilde{J}\hat{r} \times \sigma\delta(z)\hat{z}}{\sigma + i\omega\epsilon_0} \\ &= \mu_0\tilde{J}\delta(z)\hat{\phi}\end{aligned}$$

Noting that $\tilde{B}$ varies only in the $\hat{z}$ direction, equation 2.1.9 can be integrated across the boundary of the conductor, from $-\varepsilon < z < +\varepsilon$ where $\varepsilon \ll 1$.

$$\begin{aligned}\int_{-\varepsilon}^{+\varepsilon} \frac{d^2}{dz^2}\tilde{B}dz &= \int_{-\varepsilon}^{+\varepsilon} i\omega\mu_0\left(\sigma + i\omega\epsilon_0\right)\tilde{B} + \mu_0\tilde{J}\delta(z)dz \\ \frac{d}{dz}\tilde{B}^{air} - \frac{d}{dz}\tilde{B}^{conductor} &= 0 + \mu_0\tilde{J}(z=0)\end{aligned} \tag{2.2.7}$$

The magnetic field is continuous across the boundary, but the derivative of the magnetic field is not. This is not surprising since $\tilde{B}$ is constant with height above the conductor, but below the boundary it is not.

While the boundary term of magnetic diffusion equation involves the current density at the surface, the boundary term of electric diffusion equation can be seen to involve the surface charge by a simple application of Gauss' Law. This also provides quite a bit of information on what the electric boundary term does.

$$\begin{aligned}\nabla\left(\nabla \cdot \tilde{E}\right) &= \nabla\rho/\epsilon_0 \\ &= \nabla\frac{\tilde{E} \cdot \nabla\sigma}{(\sigma + i\omega\epsilon_0)}\end{aligned}$$

Rearranging some terms yields the non-trivial relation:

$$\rho = -\frac{\epsilon_0\tilde{E} \cdot \nabla\sigma}{\sigma + i\omega\epsilon_0} \tag{2.2.8}$$

Again consider the case of a uniform conductor where $\nabla\sigma = -\sigma\delta(z)\hat{z}$. Taking the limit where $\sigma \gg i\omega\epsilon_0$ and removing the time dependency, yields:

$$\rho = \epsilon_0\tilde{E}\delta(z) \tag{2.2.9}$$

which is exactly the result normally obtained for a uniform electric field over a perfect conductor. This term appears to block the diffusion of the vertical electric field into the conductor, an expected effect. This can be shown by assuming a vertically polarized electric field over a uniformly conducting surface as described in Figure 2.0.1. Integrating equation 2.1.12 twice gives:

$$\begin{aligned}\int_{-\varepsilon}^{+\varepsilon}\int \frac{d^2}{dz^2}\tilde{E}_z\, dzdz &= \int_{-\varepsilon}^{+\varepsilon}\int i\omega\mu_0\left(\sigma + i\omega\epsilon_0\right)\tilde{E}_z + \frac{d}{dz}\frac{\sigma\delta(z)}{\sigma + i\omega\epsilon_0}\tilde{E}_z\, dzdz \\ \int_{-\varepsilon}^{+\varepsilon}\frac{d}{dz}\tilde{E}_z\, dz &= \int_{-\varepsilon}^{+\varepsilon} f(z) + \frac{\sigma\delta(z)}{\sigma + i\omega\epsilon_0}\tilde{E}_z + C\, dz\end{aligned}$$

where C is an arbitrary constant and $f(z)$ is the integral of the first term of equation 2.1.12. Because both of these terms are continuous across the $z = 0$ boundary, they vanish after the definite integral giving:

$$\tilde{E}_z^{air} - \tilde{E}_z^{conductor} = \frac{\sigma}{\sigma + i\omega\epsilon_0}\tilde{E}_z(z = 0) \tag{2.2.10}$$

The vertical electric field is indeed not continuous across the boundary. In addition if $\omega \ll \sigma$, then $\sigma/(\sigma + i\omega\epsilon_0) \sim 1$ and the electric field vanishes in the conductor. For the earth, frequency components below 150 MHz satisfy $\omega \ll \sigma$, therefore these frequencies will be blocked at the surface. As will soon be shown, frequency components above 50 kHz have a very shallow skin depth and will be heavily attenuated by the conducting earth. To very good approximation, the vertical electric field in the ground is zero..

For the electric field, the boundary term effectively reduces the vertical electric field to zero. That is not the case with the magnetic field where dB/dz is discontinuous and the boundary term can be neglected in numerical solutions. Letting E_z be zero in the conductor is what is traditionally done [Jackson, 1999] and what is done in the implementation of the equations in this paper.

2.3 Solution to Uniform Diffusion Equations in Cartesian Coordinates

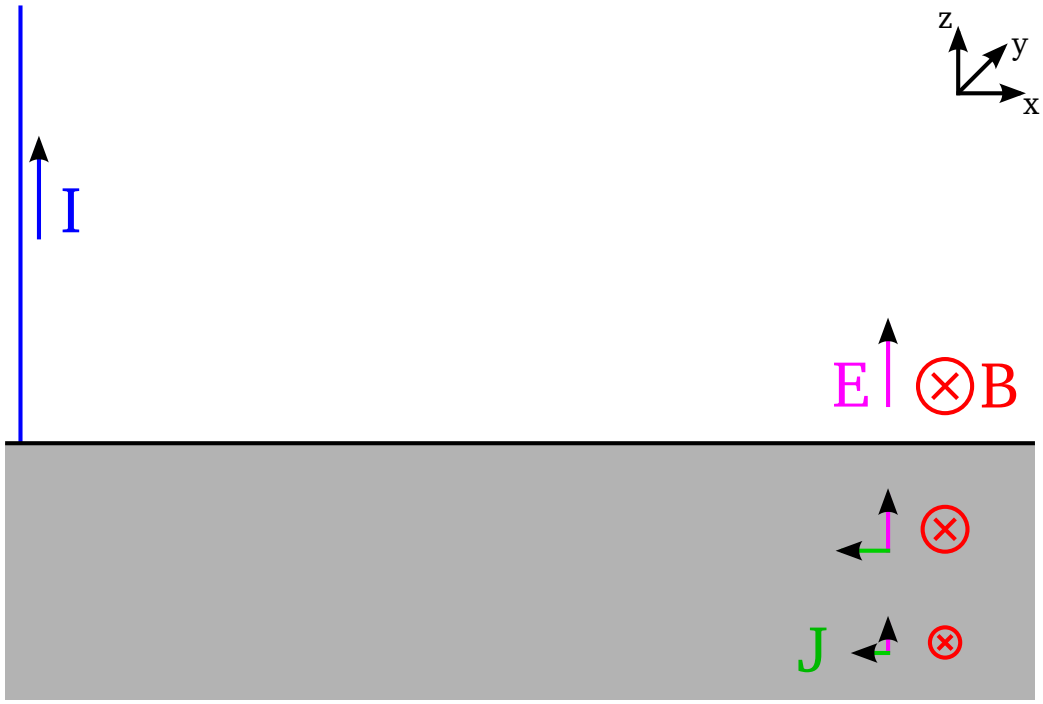

Figure 2.3.1: A Cartesian representation of the problem described in Figure 2.0.1. The vertical lightning channel to ground is far off in the $-\hat{x}$ direction. This means that there is a magnetic field in the $\hat{y}$ direction and an electric field in the $+\hat{z}$ direction above the conductor. Inside the conductor, the spatial gradient of the magnetic field will induce a current density in the $-\hat{x}$ direction.

The formulation presented earlier was independent of choice of coordinate system, but Figure 2.0.1 describes a problem with azimuthal symmetry. This problem lends itself particularly well to a cylindrical coordinate system. Far from the current channel the fields become effectively rectangular, allowing a Cartesian coordinate system to be used.

Let the current in the channel be pointing in the $+\hat{z}$ direction (negative CG) and be located far in the $-\hat{x}$ direction. In this case, the magnetic field is in the $+\hat{y}$ direction, and the electric field is in the $+\hat{z}$ direction. Far from the current channel, the magnetic and electric

fields will be uniform in the $\hat{x}$ and $\hat{y}$ directions; neglecting the boundary term equation 2.1.13 simplifies to:

$$\frac{\partial^2 \tilde{F}}{\partial z^2} = i\omega\mu_0\sigma\tilde{F}$$

For the magnetic field, this has a solution:

$$\tilde{B} = \tilde{B}_{z_0} e^{\pm\sqrt{i\omega\mu_0\sigma}(z-z_0)}$$

where $\tilde{B}_{z_0}$ is the field at $z = z_0$. Noting that $\sqrt{i} = (1+i)/\sqrt{2}$ and introducing the skin depth[2] $\delta = \sqrt{2/\omega\mu_0\sigma}$ yields:

$$\begin{aligned} \tilde{B} &= \tilde{B}_{z_0} e^{\pm(1+i)\sqrt{\omega\mu_0\sigma/2}(z-z_0)} \\ \tilde{B} &= \tilde{B}_{z_0} e^{(1+i)(z-z_0)/\delta} \end{aligned} \tag{2.3.1}$$

To obtain a physical solution, the field needs to go to zero at $z = -\infty$, which is why only the positive exponential is kept in the final solution.

Since the solution for $\tilde{B}$ is already in the frequency domain, that is $\tilde{B} = \tilde{B}(\omega, z)$, the transfer function for the magnetic field is simply:

$$\tilde{T}(\omega, z) = e^{(1+i)(z-z_0)/\delta} \tag{2.3.2}$$

shown in Figure 2.3.2a. Equation 2.3.2 describes a strong low pass filter. Ground with a resistivity of 100 $\Omega \cdot$ m will attenuate a 50 kHz signal by 10 dB by a depth of 100 m (the depth of the Sago mine).

Because the $\tilde{H}$, $\tilde{E}$ and $\tilde{J}$ are all governed by the same differential equation if boundary terms are neglected, the same transfer function holds for all fields. However, the boundary condition for the horizontal electric, $\tilde{E}_x$, field is not known at the surface. The horizontal electric

[2] δ was used previously to denote a Dirac delta function. In this paper, δ is also used to denote the skin depth. Unless it is specifically stated, δ refers to the skin depth and not a Dirac delta function.

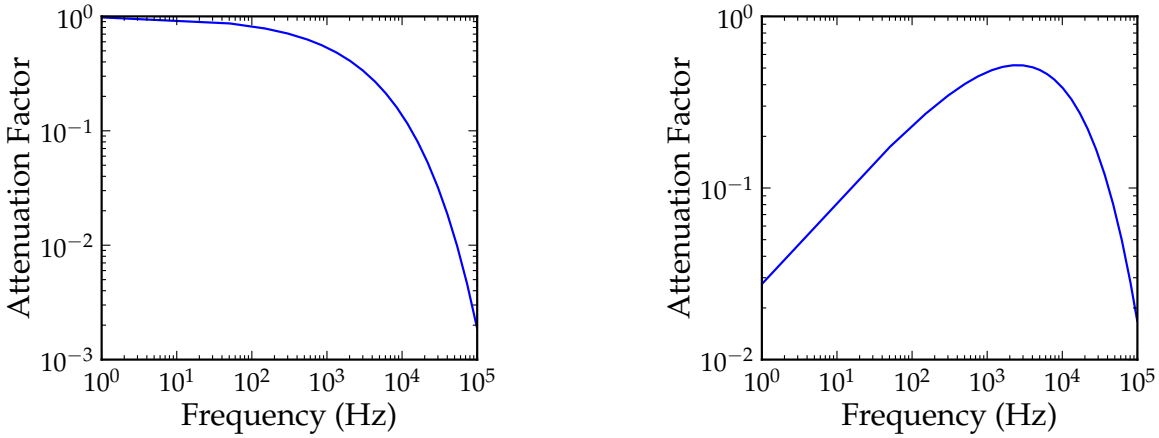

(a) Magnetic Field

(b) Electric Field

Figure 2.3.2: Frequency of the magnetic and electric field using a resistivity of 100 $\Omega \cdot$ m and a depth of 100 m. (a) Magnitude of $\tilde{B}_y / \tilde{B}_{z_0}$ (equation 2.3.2). (b) Magnitude of $\tilde{E}_x / \tilde{H}_y$ (equation 2.3.3).

field in the ground can be calculated from the vertical gradient of the magnetic field which will give rise to an electric field in the $-\hat{x}$ direction. Using Ampére's Law (equation 2.1.6):

$$\begin{aligned}
\nabla \times \tilde{B} &= \mu_0 \left(\sigma + i\omega\epsilon_0\right) \tilde{E} \\
-\frac{\partial \tilde{B}_y}{\partial z} &= \mu_0 \sigma \tilde{E}_x \quad \text{Assuming } \omega \ll \sigma/\epsilon_0 \\
-\frac{\partial}{\partial z} \tilde{B}_{z_0} e^{(1+i)(z-z_0)/\delta} &= \mu_0 \sigma \tilde{E}_x \\
-\frac{1+i}{\delta} \tilde{B}_{z_0} e^{(1+i)(z-z_0)/\delta} &= \mu_0 \sigma \tilde{E}_x \\
\tilde{E}_x &= -\frac{1+i}{\delta \mu_0 \sigma} \tilde{B}_{z_0} e^{(1+i)(z-z_0)/\delta}
\end{aligned}$$

which can be further simplified by substituting for the skin depth δ.

$$\begin{aligned}
\tilde{E}_x &= -\frac{1+i}{\mu_0 \sigma \sqrt{2/\omega\mu_0\sigma}} \tilde{B}_{z_0} e^{(1+i)(z-z_0)/\delta} \\
\tilde{E}_x &= -(1+i)\sqrt{\frac{\omega}{2\mu_0\sigma}} \tilde{B}_{z_0} e^{(1+i)(z-z_0)/\delta} \qquad (2.3.3)
\end{aligned}$$

The prefactor term can be treated as part of the transfer function for the horizontal electric field when the conductivity is uniform, but this is not an accurate description and causes trouble

for more complex conductivity profiles. A more accurate description is that the prefactor term gives the horizontal electric field at the surface. That is:

$$-(1+i)\sqrt{\frac{\omega}{2\mu_0\sigma}}\tilde{B}_y(z_0) \;=\; \tilde{E}_x(z_0) \tag{2.3.4}$$

The prefactor converts the magnetic field at the surface to electric field at the surface, and is frequency dependent. Because of this, the frequency response for the horizontal electric field looks like a band-pass filter, as seen in Figure 2.3.2b.

Since there is a non-zero horizontal electric field inside a conductor, there should be a non-zero current density as well from Ohm's Law. Setting $z_0 = 0$;

$$\tilde{J} \;=\; -(1+i)\sqrt{\frac{\sigma\omega}{2\mu_0}}\tilde{B}_0 e^{(1+i)z/\delta}\hat{x} \tag{2.3.5}$$

This current density is pointing in the $-\hat{x}$ direction, towards the lightning channel, required for conservation of charge. Because charge is conserved, the total current of the lightning channel can be calculated by:

$$\tilde{I} \;=\; \oint_S \tilde{J}\cdot dA$$

where the surface S is depicted in Figure 2.0.1. Far from the lightning channel, the Cartesian coordinates can be rotated around the surface such that $\hat{y}$ always points in the $\hat{p}hi$ direction and $\hat{x}$ points in the $\hat{r}$ direction. To be able to calculate this surface integral, the magnetic field at the surface must be known. In the magnetostatic limit the magnetic field produced by an infinite line current is $\tilde{B}_0 = \mu_0\tilde{I}/2\pi R\ \hat{\phi}$, where R is the distance from the lightning strike. In which case the current density becomes

$$\tilde{J} \;=\; -(1+i)\sqrt{\frac{\sigma\mu_0\omega}{2}}\frac{\tilde{I}}{2\pi R}e^{(1+i)z/\delta}\hat{x}$$

The surface integral can now be calculated directly

$$\begin{aligned}
\tilde{I} &= \oint_S -(1+i)\sqrt{\frac{\sigma\mu_0\omega}{2}}\frac{\tilde{I}}{2\pi R}e^{(1+i)z/\delta}\hat{r}\cdot dA \\
\tilde{I} &= 2\pi R\int_0^{-\infty} -\frac{1+i}{\delta}\frac{\tilde{I}}{2\pi R}e^{(1+i)z/\delta}dz \quad \text{Using azimuthal symmetry} \\
\tilde{I} &= -\tilde{I}\frac{1+i}{\delta}\frac{\delta}{1+i}\, e^{(1+i)z/\delta}dz\Big|_0^{-\infty} \\
\tilde{I} &= \tilde{I}
\end{aligned}$$

In the magnetostatic limit the surface integral of $\tilde{J}$ gives exactly the expected total current in the lightning channel.

2.4 Solution to Uniform Diffusion Equations in Cylindrical Coordinates

The geometry of the problem described in Figure 2.0.1 lends itself particularly well to cylindrical coordinates. Solving equation 2.1.13 in cylindrical coordinates is more complicated because the Laplacian operator has more terms. For a scalar, it is given by:

$$\nabla^2 f = \frac{1}{r}\frac{\partial}{\partial r}\left(r\frac{\partial f}{\partial r}\right) + \frac{1}{r^2}\frac{\partial^2 f}{\partial \phi^2} + \frac{\partial^2 f}{\partial z^2} \tag{2.4.1}$$

For a vector, the terms in pointing in the radial, azimuthal, and vertical directions are not the same [Arfken, 1985]:

$$\begin{aligned}\vec{\nabla}^2\vec{A} &= \left(\nabla^2 A_r - \frac{1}{r^2}A_r - \frac{2}{r^2}\frac{\partial A_\phi}{\partial \phi}\right)\hat{r} \\ &+ \left(\nabla^2 A_\phi - \frac{1}{r^2}A_\phi + \frac{2}{r^2}\frac{\partial A_r}{\partial \phi}\right)\hat{\phi} \\ &+ \left(\nabla^2 A_z\right)\hat{z}\end{aligned} \tag{2.4.2}$$

where $\vec{\nabla}^2$ is used to differentiate the vector Laplacian from the scalar Laplacian. While the diffusion equation for the vertical electric field is unchanged, there is an additional term for the azimuthal magnetic field and radial electric field. Assuming the magnetic field is azimuthally symmetric and of the form $\tilde{B} = B_\phi(\omega, r, z)\hat{\phi}$, then the differential equation for the uniform diffusion equation becomes:

$$\begin{aligned}\vec{\nabla}^2\tilde{B} &= \left(-\frac{2}{r^2}\frac{\partial B_\phi}{\partial \phi}\right)\hat{r} + \left(\nabla^2 B_\phi - \frac{1}{r^2}B_\phi\right)\hat{\phi} \\ &= \nabla^2 B_\phi - \frac{1}{r^2}B_\phi\,\hat{\phi} \\ \nabla^2 B_\phi - \frac{1}{r^2}B_\phi &= i\omega\mu_0\left(\sigma + i\omega\epsilon_0\right)B_\phi \\ \frac{1}{r}\frac{\partial}{\partial r}\left(r\frac{\partial B_\phi}{\partial r}\right) + \frac{1}{r^2}\frac{\partial^2 B_\phi}{\partial \phi^2} + \frac{\partial^2 B_\phi}{\partial z^2} - \frac{1}{r^2}B_\phi &= i\omega\mu_0\left(\sigma + i\omega\epsilon_0\right)B_\phi \\ \frac{1}{r}\frac{\partial}{\partial r}\left(r\frac{\partial B_\phi}{\partial r}\right) + \frac{\partial^2 B_\phi}{\partial z^2} - \frac{1}{r^2}B_\phi &= \left(i\omega\mu_0\sigma - k^2\right)B_\phi\end{aligned} \tag{2.4.3}$$

where $k = \omega/c$ in due to the displacement current. Earlier this term was neglected because it was very small in comparison with the conductivity. Here it must be reintroduced to get the differential equation in a form that has a known solution. To further simplify this equation, separation of variables techniques can be used by assuming B_ϕ is of the following form,

$$\tilde{B}_\phi(\omega, r, z) \equiv \tilde{Z}(\omega, z)\tilde{R}(\omega, r) \tag{2.4.4}$$

where Z expresses the vertical dependence of B_ϕ and R expresses the radial dependance of B_ϕ. Applying equation 2.4.4 to equation 2.4.3 gives:

$$\begin{aligned} ZR'' + \frac{1}{r}ZR' + RZ'' - \frac{1}{r^2}ZR &= \left(i\omega\mu_0\sigma - k^2\right)ZR \\ \frac{R''}{R} + \frac{R'}{rR} + \frac{Z''}{Z} - \frac{1}{r^2} &= \left(i\omega\mu_0\sigma - k^2\right) \end{aligned}$$

which separates into the following two ODE's

$$r^2R'' + rR' + \left(r^2k^2 - 1\right)R = 0 \tag{2.4.5}$$

$$Z'' - i\omega\mu_0\sigma Z = 0 \tag{2.4.6}$$

Equation 2.4.5 is Bessel's equation and equation 2.4.6 is the same equation obtained in the Cartesian case. These have the following solutions (neglecting normalization constants):

$$R(r) = H_1^{(1)}(rk) \tag{2.4.7}$$

$$Z(z) = e^{(1+i)z/\delta} \tag{2.4.8}$$

where $H_1^{(1)}$ is a Hankel function of the first kind of order 1 and $\delta = \sqrt{2/\omega\mu_0\sigma}$ is the same skin depth seen before. The solutions involving the Hankel function of the second kind are not physical. Only the Hankel function of the first kind has solutions propagating in the $+\hat{r}$ direction. This solution holds for the horizontal electric field as well, since there is no electric field in the $\hat{\phi}$ direction.

The solution for vertical electric field is similar, except that the separated differential equations are

$$r^2R'' + rR' + \left(r^2k^2\right)R = 0 \tag{2.4.9}$$

$$Z'' - i\omega\mu_0\sigma Z = 0 \tag{2.4.10}$$

which have solutions

$$R(r) = H_0^{(1)}(rk) \tag{2.4.11}$$

$$Z(z) = e^{(1+i)z/\delta} \tag{2.4.12}$$

where $H_0^{(1)}$ is a Hankel function of the first kind of order 0.

The radial solutions for the magnetic and vertical electric fields are not quite the same. Because the radial and vertical solutions for both the electric and magnetic field are independent of each other, the radial solution can be neglected. In addition, the vertical transfer function in cylindrical is identical to the transfer function obtained using Cartesian coordinates. This means that there is no need to work with the more complicated cylindrical Laplacian operator.

2.5 Discussion

In Section 2.1 the general form of the diffusion equations was derived, keeping terms for the displacement current and allowing gradients in the conductivity. The resulting equations 2.1.9 and 2.1.12 are fully general, and apply to much more than the electric and magnetic field produced by a vertical lightning channel. For the vertical electric field, the boundary term involving $\nabla\sigma$ will cause the electric field to not penetrate deeply into the ground. This is expected, since the vertical electric field will induce a surface charge on the conductor which will cancel out the field inside the conductor. For the magnetic field, the boundary term causes only

a discontinuity in $\partial B/\partial z$. This means that the magnetic field will penetrate into the conductor. Because there is a vertical gradient to the magnetic field, there is also an induced horizontal electric field which also penetrates the conductor.

Ignoring gradients in conductivity, the electric and magnetic fields follow the following diffusion equation:

$$\nabla^2 \tilde{F} = i\omega\mu_0 \left(\sigma + i\omega\epsilon_0\right) \tilde{F} \tag{2.1.14}$$

where F is any of the above. The same holds for the current density $\tilde{J}$ because σ is assumed to be constant. If there are no gradients in permeability μ, the above equation also holds for the auxiliary field $\tilde{H}$.

In Sections 2.3 and 2.3, the diffusion equation is solved in Cartesian and cylindrical coordinates. In the cylindrical case, the vertical solution decouples from the radial solution. This is important, it means that radial solution can be ignored when finding the field in the ground if the field at the surface is known. In both cases, the vertical solution is the same:

$$\tilde{F} = \tilde{F}_{z_0} e^{(1+i)(z-z_0)/\delta} \tag{2.3.1}$$

where $\delta = \sqrt{2/\omega\mu_0\sigma}$ is the skin depth and $\tilde{F}$ is the electric or magnetic field. The horizontal electric field can be calculated from the change of $\tilde{B}$ with depth. This gives:

$$\tilde{E}_x = -(1+i)\sqrt{\frac{\omega}{2\mu_0\sigma}}\tilde{B}_{z_0} e^{(1+i)(z-z_0)/\delta}\hat{x} \tag{2.3.3}$$

Using equations 2.3.1 and 2.3.3, finding the fields in the Sago mine is straight forward if the magnetic field at the surface is known. Details on the exact process used to do this is given in Appendix A.

CHAPTER 3

LIGHTNING MODELS

Using the solutions presented in Chapter 2, it is possible to calculate the fields produced below ground by diffusion given the field at ground level. Of particular interest is application of the diffusion equations to fields that might be produced by lightning. In the ideal situation, the fields produced by a lightning strike are directly measured, however direct field measurement of the magnetic field over the Sago mine are not available. Long range sensor networks, such as NLDN, were operational at the time, giving the location of the lightning strikes near the mine and estimates of the peak current.

In this chapter some simple methods are developed for numerically estimating the magnetic field produced by a lightning flash given the peak current. A vertical lightning strike will produce a vertical electric field and an azimuthal magnetic field. As discussed before, the vertical electric field will be quickly shielded by induced surface charge and so can be neglected. The fields produced by a lightning return stroke can be modeled as being produced by a current pulse traveling up a conducting channel into the cloud as indicated in Figure 3.1.1. The channel is several kilometers long, and the current pulse is assumed to be roughly triangular with a duration of tens of microseconds and a peak amplitude of tens of kiloamps [Uman et al., 1974]. The pulse travels up the channel at a significant fraction of the speed of light, between 1×10^8 and $2 \times 10^8 \mathrm{m/s}$ [Rakov & Uman, 2003, Uman, 1969].

To implement a model of a lightning return stroke, some approximations must be made. The parameters shown in Table 3.1 are used as the input for all the models developed in this

Channel Length	7 km
Current Pulse Rise Time	2 μs
Current Pulse Fall Time	48 μs
Current Pulse Duration	50 μs
Current Pulse Amplitude	10 kA
Current Pulse Velocity	1×10^8 m/s
Ground Conductivity	∞

Table 3.1: A table of the parameters used for the all lightning return stroke models presented here.

chapter; some models do not use all parameters. To simplify the calculations, the effects of a continuing current are neglected and the ground is treated as a perfect conductor. Assuming the ground is a perfect conductor may seem at odds with calculating the fields in the ground because if the ground is a perfect conductor the magnetic field will be canceled out in the ground by a surface current. However, the purpose of these models is to estimate the fields at the surface so that they may be used as boundary conditions for the diffusion equations. The propagation speed of the electric and magnetic fields horizontally away from the return stroke is much faster than the speed of downward diffusion, therefore assuming the ground is a perfect conductor is sufficient.

From just the parameters in Table 3.1 it is possible to make a rudimentary prediction about the fields produced by a lightning return stroke. At the speed $v = 1 \times 10^8$ m/s, the current pulse will take 70 μs to travel the 7 km length of the return stroke channel. Close to the channel it can take as much as an additional 23 μs for radiation produced at the top of the channel to reach the observation point P due to the finite speed of light. Therefore, the total duration of the fields produced by the return stroke itself should be on the order of 100 μs.

Six models of increasing complexity will be developed in this chapter and are summarized in Table 3.2. The first 3 models are based on a magnetostatic approximation and give a good first order estimate of the amplitude of the magnetic field produced by a return stroke.

	Model	Description	Length	Velocity	Page
Magnetostatic	1	Infinite Line Current	∞	∞	p. 28
	2	Finite Line Current	Finite	∞	p. 29
	3	Transmission Line Current	Finite	Finite	p. 30
Electrodynamic	4a	Infinite Line Current with Step Input	∞	∞	p. 36
	4b	Infinite Line Current with Ramp Input	∞	∞	p. 39
	5	Finite Line Current	Finite	∞	p. 44
	6a	Transmission Line Current	Finite	Finite	p. 50
	6b	Simplified Transmission Line Current	Finite	Finite	p. 53

Table 3.2: A summary of the models described in this chapter. Length refers to the length of the vertical return stroke channel. Velocity refers to the velocity of the current pulse up the channel.

The magnetostatic models do not allow for a propagation delay between the return stroke channel and the observation point P. Because the duration of the current pulse is on the same order as the delay time from the return stroke to the observation point P, 3 electrodynamic models are then developed. Model 6, the most complete model, allows the current pulse to travel up the return stroke channel at a finite velocity [Uman et al., 1974].

3.1 Magnetostatic Models

To begin the models, we will assume that the current changes slowly with time and that effects of propagation delays between the return stroke channel and the observation point, P, can be neglected. The magnetostatic models are significantly easier to understand than the electrodynamic models; they provide physical insight to the problem and provide a good first order approximation to the magnetic fields produced by a lightning return stroek. In addition, the electrodynamic models should reduce to the magnetostatic models in the limit of a slowly changing current.

3.1.1 Model 1: Infinite Length Line Current

The simplest model of a return stroke is to assume the current channel is infinitely long and that the current is flowing simultaneously along the entire channel. Because the ground is assumed to be a perfect conductor, there is an image current below the surface traveling in the same direction. This means that the current channel extends from $z = -\infty$ to $z = +\infty$. Figure 3.1.1 depicts the basic geometry of the system. The magnetostatic form of Ampére's Law then gives:

$$\nabla \times \vec{B} \;=\; \mu_0 \vec{J}$$

In integral form this becomes

$$\oint \vec{B} \cdot d\ell \;=\; \mu_0 I_{enc}$$

Since the magnetic field is azimuthally symmetric with the form $\vec{B} = B_\phi \hat{\phi}$, this line integral is particularly easy to solve, giving the well known solution

$$B_\phi = \frac{\mu_0 I}{2\pi r}\,, \tag{3.1.1}$$

where I is the current of the lightning channel and r is the radial distance from the current channel, as depicted in Figure 3.1.1. The peak current for a typical lightning strike is on the order of 10 kA. At a distance of 1 km, this gives a magnetic field of approximately 1.7 A/m. This agrees quite well with measured fields on the order of a few A/m.

For the electric field Gauss' law gives:

$$\nabla \cdot \vec{E} \;=\; \frac{\rho}{\epsilon_0} \tag{3.1.2}$$

There is charge in the cloud which changes slowly with time, giving a static vertical electric field which is not discussed in these models. If the current channel is not charge neutral, according to equation 3.1.2 there is a radial horizontal electric field. However because the ground

is assumed to be a perfect conductor, this tangential electric field vanishes at the surface. For the vertical electric field, Faraday's law gives:

$$\begin{aligned} \nabla \times \vec{E} &= -\frac{\partial \vec{B}}{\partial t} \\ -\frac{\partial E_z}{\partial r} &= -\frac{\mu_0}{2\pi r}\frac{\partial I}{\partial t} \end{aligned} \tag{3.1.3}$$

Integrating with respect to r gives the unexpected result that $E_z \propto \ln(r/r_0)$! Not only is r_0 not well defined, but E_z *increases* with distance. While the magnetostatic approximation above gave a reasonable result for the magnetic field, the results for the electric field are unphysical. While a magnetostatic approximation will produce estimates of the magnetic field, a fully electrodynamic model will be required to get estimates for the electric field.

3.1.2 Model 2: Finite Length Line Current

Lightning channels are not infinitely long, and as the distance to the strike increases, assuming they are becomes less and less valid. To find the magnetic field produced by a finite length lightning channel, one must integrate the differential magnetic field along the channel [Uman, 1987]. The magnetic field produced by a current of length dz is:

$$\begin{aligned} d\vec{B} &= \frac{\mu_0 I}{4\pi \text{ɾ}^2}\vec{dz} \times \hat{\text{ɾ}} \\ &= \frac{\mu_0 I}{4\pi \text{ɾ}^2}\sin(\theta) dz \hat{\phi} \end{aligned} \tag{3.1.4}$$

where ɾ is the distance from the current element to the observation point P, and θ is the angle between the current channel and $\vec{\text{ɾ}}$. From Figure 3.1.1, $\sin(\theta)$ can be seen to be $r/\text{ɾ}$, and with $\text{ɾ} = \sqrt{z^2 + r^2}$, equation 3.1.4 becomes:

$$d\vec{B} = \frac{\mu_0 I}{4\pi}\frac{r}{(z^2 + r^2)^{3/2}} dz \hat{\phi} \tag{3.1.5}$$

The total magnetic field can be found by integrating and multiplying by 2 to account for the image current, giving:

$$\begin{aligned} B_\phi &= 2\frac{\mu_0 I}{4\pi}\int_{z_1}^{z_2}\frac{r}{(z^2+r^2)^{3/2}}dz \\ &= 2\frac{\mu_0 I r}{4\pi}\left.\frac{z}{r^2\sqrt{z^2+r^2}}\right|_{z_1}^{z_2} \\ &= \frac{\mu_0 I}{2\pi r}\left(\frac{z_2}{\sqrt{z_2^2+r^2}}-\frac{z_1}{\sqrt{z_1^2+r^2}}\right) \end{aligned} \tag{3.1.6}$$

If this current extends from the ground to a height H as in a cloud-to-ground strike, this becomes:

$$B_\phi = \frac{\mu_0 I}{2\pi r}\frac{H}{\sqrt{H^2+r^2}} \tag{3.1.7}$$

For small r, equation 3.1.7 reduces to the same result obtained for an infinite channel. For intermediate distances, the magnetic field is reduced because $H/\sqrt{H^2+r^2} < 1$. In the case that $r \gg H$, equation 3.1.7 becomes:

$$B_\phi = \frac{\mu_0 I}{2\pi r}\frac{H}{r} \tag{3.1.8}$$

which falls off faster with distance than model 1 because far away from the lightning strike, the current channel starts to look like a point source.

3.1.3 Model 3: Finite Length Transmission Line Current

Models 1 and 2 assume the current is assumed to be changing slowly with time and varying simultaneously along the channel. A more accurate description is that a current pulse travels from the bottom of the current channel to the top at a constant velocity, as if the current channel is a transmission line. To treat this, the current is assumed to be a function of ξ, where

$\xi = t - z/v$ in the case of a transmission line. Because the current is now a function of z, equation 3.1.5 becomes:

$$B_\phi = \frac{\mu_0}{2\pi} \int_0^H I(t - z/v) \frac{r}{(z^2 + r^2)^{3/2}} dz \, . \tag{3.1.9}$$

This happens to have the same form as the inductive term of model 6a, which is exploited in the simplification presented in model 6b.

The integral in equation 3.1.9 can not be evaluated unless $I(\xi)$ is known. To evaluate equation 3.1.9 for an arbitrary current pulse, first it is solved for a simple form of $I(\xi)$. A good choice for the simple form of the current is a step function, $I(\xi) = I_0 u(\xi)$: [1]

$$I(\xi) = \begin{cases} 0 & \xi < 0 \\ I_0 & \xi > 0 \end{cases} . \tag{3.1.10}$$

The magnetic field for any slowly changing current waveform traveling up the lightning channel can be modeled as a sequence of step functions like a digital signal. Using a step function for the current, equation 3.1.9 becomes:

$$\begin{aligned} B_\phi &= \frac{\mu_0 I_0}{2\pi} \int_0^H u(t - z/v) \frac{r}{(z^2 + r^2)^{3/2}} dz \\ &= \frac{\mu_0 I_0}{2\pi} \int_0^{vt} \frac{r}{(z^2 + r^2)^{3/2}} dz \\ &= \frac{\mu_0 I_0}{2\pi r} \frac{z}{\sqrt{z^2 + r^2}} \Bigg|_0^{vt} \\ &= \begin{cases} \frac{\mu_0 I_0}{2\pi r} \frac{vt}{\sqrt{(vt)^2 + r^2}} & t < H/v \\ \frac{\mu_0 I_0}{2\pi r} \frac{H}{\sqrt{(H)^2 + r^2}} & t > H/v \end{cases} \end{aligned} \tag{3.1.11}$$

The magnetic field of a single step starts at zero and then increases linearly with time. If the current line is infinite, then with increasing time the step response asymptotically approaches

[1] $u(t)$ is a Heaviside step function, 0 for $t < 0$ and 1 for $t > 0$. $u(t) = \int \delta(t) dt$ where $\delta(t)$ is the Dirac delta function.

the magnetic field of model 1. If the current line is finite, the increase ceases once the current reaches the top of the channel.

Figure 3.1.2 shows a comparison of the all the magnetostatic models using the triangular current shown in Figure 3.1.2a as the input. Figure 3.1.2b-f compares the magnetic field waveforms for models 1-3 at various ranges. In models 1 and 2 the magnetic field is proportional to the current. Near the current channel, models 1 and 2 produce almost identical magnetic fields. With increasing distance, the amplitude of the field produced by model 2 becomes significantly smaller than model 1 as expected.

The results from model 3 give much more realistic magnetic field waveforms than models 1 or 2. The magnetic fields produced by model 3 are longer in duration and smaller in amplitude than both models 1 and 2. The magnetic field waveforms of model 3 are also smooth, lacking discontinuities in $\partial B/\partial t$ except at $t = 70\mu$s. The discontinuity at 70μs is caused when the current pulse reaches the top of the lightning channel and artificially turns off. Because the delay associated with finite propagation speed was not accounted for in any of the magnetostatic models, the magnetic fields in all models start at $t = 0$ instead of the expected $t = r/c$. In addition, close to the channel the time delay from the top of the channel is significantly different than from the bottom of the channel, which will distort the magnetic field. These effects will be taken into account in the electro dynamic models of Section 3.2.

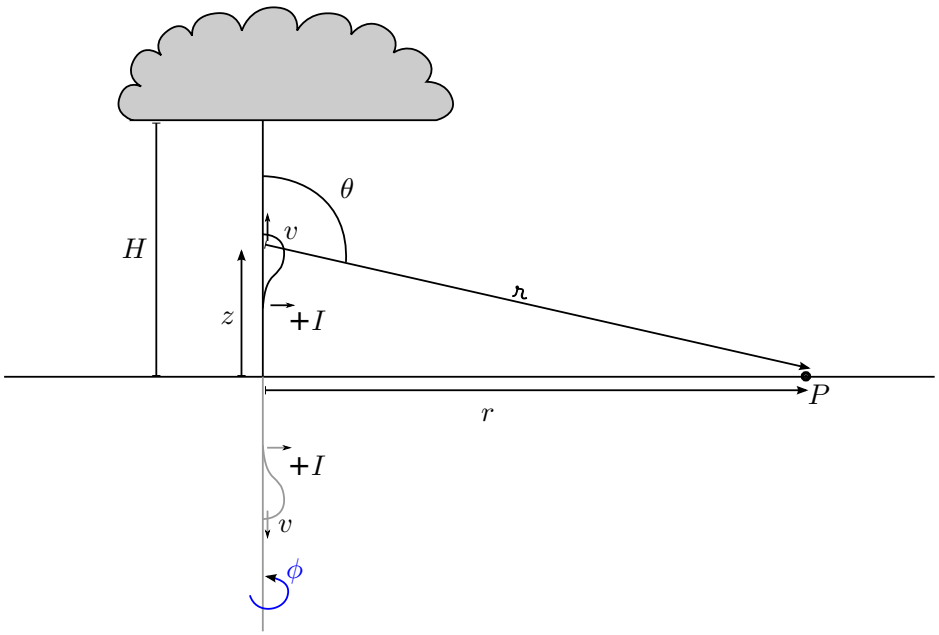

Figure 3.1.1: A current pulse travels up a conducting channel of height H at velocity v over a perfect conductor. r and ϕ are the cylindrical coordinate vectors of the point P. $\wr$ is a vector from the current element to observation point P which varies with position along the channel. θ is the angle between the vertical channel and the vector $\wr$. This diagram shows a spatially short current pulse, however a 50μs long pulse traveling at 1×10^8m/s is 5km long.

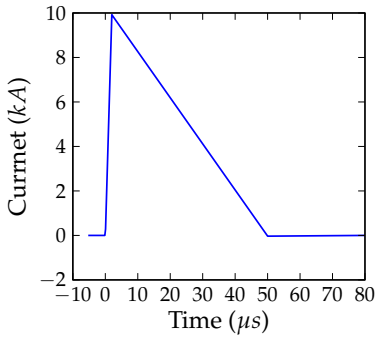

(a) Current

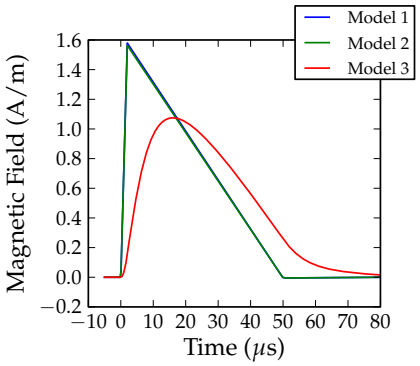

(b) 1km

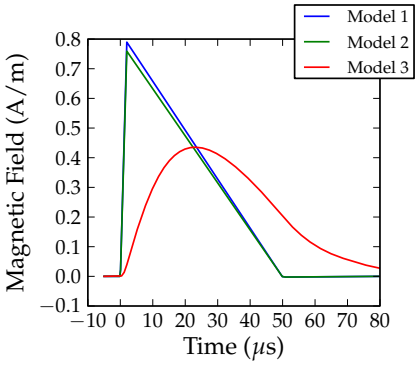

(c) 2km

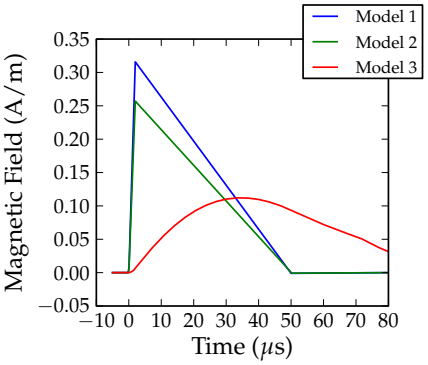

(d) 5km

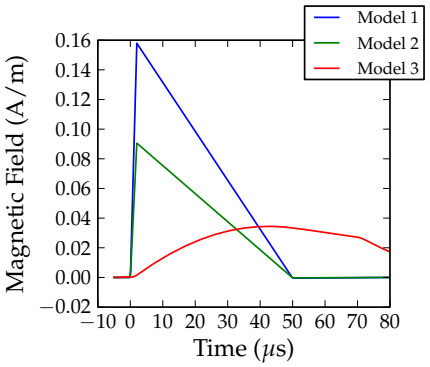

(e) 10km

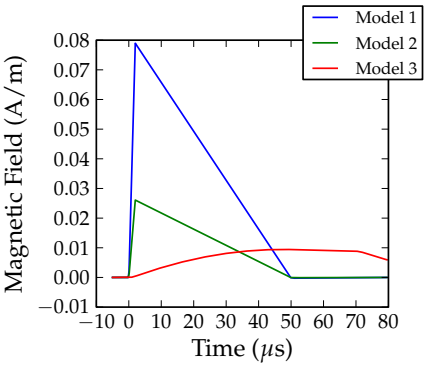

(f) 20km

Figure 3.1.2: A comparison of the magnetostatic lightning models for a triangular input current shown in (a); models 1-3 at various distances from the lightning channel (b-f).

3.2 Electrodynamic Models

Because the duration of the current pulse is on the same order as the propagation delay between the channel and the observation point P, a fully electrodynamic model is required to accurately model a lightning return stroke[2]. The most direct way to approach the electrodynamic problem is to solve for the vector and scalar potentials, and then use these to obtain the electric and magnetic fields. For a vertical line current at the origin, the vector potential is:

$$\vec{A}(r,t) = \frac{\mu_0}{4\pi}\int \frac{\vec{I}(t-\text{ɲ}/c,z)}{\text{ɲ}}dz \tag{3.2.1}$$

where ɲ is a vector from the observation point P to the current, and $t-\text{ɲ}/c$ is the retarded time, t_r. In general, the current can have any functional dependence on t_r and z. However, in all the models presented in this chapter the current can be described as a function of a single variable, ξ, where ξ is a function of t_r and z which is model dependent. In this case, the vector potential is given by:

$$\vec{A}(r,t) = \frac{\mu_0}{4\pi}\int \frac{\vec{I}(\xi)}{\text{ɲ}}dz \tag{3.2.2}$$

The fields can then be calculated from the vector potential as:

$$\vec{E} = -\frac{\partial \vec{A}}{\partial t} - \nabla\Phi \tag{3.2.3}$$

$$\vec{B} = \nabla \times \vec{A} \tag{3.2.4}$$

where the scalar potential, Φ, must also be known to calculate the electric field.

To implement determining electric and magnetic fields from complex current waveforms, first the field will be determined for a simple waveform such as a step function. Then other current waveforms such as the triangular waveform described in Table 3.1 can be formed

[2] An additional benefit of an electrodynamic model is that it will produce more reasonable vertical electric field amplitudes, even though the vertical electric field will not penetrate the ground.

by superimposing many of these simple shapes. For example, an arbitrary input current can be modeled as the superposition of a number of step functions, similar to a digitized signal[3].

To develop an electrodynamic model, we will follow the same basic approach as in Section 3.1. Namely, in model 4, we will solve for and implement the fields for the case of an infinite line current where the current changes simultaneously along the channel. Model 5 is the same as model 4, but the line current is restricted to a finite length. Assuming the current changes simultaneously all along the current is not a good assumption when including the effects of a propagation delay. This is because the speed the current travels up the channel is comparable to the speed of light. For this reason, the results of models 4 and 5 do not provide accurate models of lightning. In model 6 the propagation of the current pulse up the channel is also treated by modeling the current channel as a transmission line.

3.2.1 Model 4a: Infinite Length Line Current with a Step Input

The simplest electrodynamic model is that of an infinite line where the entire line is excited simultaneously with a step function, meaning ξ has no z dependence and $I(\xi) = I_0 u(t - \text{ɾ}/c)$. This problem is outlined on page 425 of Griffiths' Introduction to Electrodynamics [Griffiths, 1989] and is reproduced here with some added detail. In this case, the vector potential in equation 3.2.2 becomes:

$$\vec{A}(r,t) = \frac{\mu_0 I_0}{4\pi} \int_{-\infty}^{+\infty} \frac{u(t - \text{ɾ}/c)}{\sqrt{r^2 + z^2}} \hat{z}\, dz \tag{3.2.5}$$

The line current turns on instantly at all points along the line at $t = 0$, but news of this does not reach observation point P until $t \geq \text{ɾ}/c$. Therefore an observer at point P will not see the entire current channel, and the limits of integration are restricted to $-z_m < z < z_m$ where

[3]As will be shown in Section 3.2.1, using step functions to build the current waveforms doesn't work for the electrodynamic models like it did in model 3. In the electrodynamic models, the simple shape must also have a finite time derivative.

$z_m = \sqrt{(ct)^2 - r^2}$. Because the integral is also symmetric about $z = 0$, we can integrate from $0 \rightarrow z_m$ and multiply by 2,

$$\begin{aligned} A_z(r,t) &= 2\frac{\mu_0}{4\pi}\int_0^{z_m}\frac{I_0 dz}{\sqrt{r^2+z^2}} \\ &= \frac{\mu_0 I_0}{2\pi}\ln\left(z+\sqrt{r^2+z^2}\right)\Big|_0^{\sqrt{(ct)^2-r^2}} \\ &= \frac{\mu_0 I_0}{2\pi}\ln\left(\frac{ct+\sqrt{(ct)^2-r^2}}{r}\right) \end{aligned} \tag{3.2.6}$$

The magnetic field can be calculated by taking the curl

$$\begin{aligned} \vec{B} &= \nabla\times\vec{A} = -\frac{\partial}{\partial r}\vec{A}\hat{\phi} \\ B_\phi &= -\frac{\mu_0 I_0}{2\pi}\frac{-(r'+ct)/r^2 - 1/r'}{(r'+ct)/r} \\ &= \frac{\mu_0 I_0}{2\pi r}\frac{(r'+ct)+r^2/r'}{(r'+ct)}\frac{(ct-r')}{(ct-r')} \\ &= \frac{\mu_0 I_0}{2\pi r}\frac{D^2+(ct-r')r^2/r'}{r^2} \\ &= \frac{\mu_0 I_0}{2\pi r}\frac{ct}{\sqrt{(ct)^2-r^2}} \end{aligned} \tag{3.2.7}$$

As $t \rightarrow \infty$ for a single step, the solution becomes equation 3.1.1, the result from model 1.

To calculate the electric field, the scalar potential must be known. For an actual lightning strike, the scalar potential is not zero since there is physical charge separation in the storm that created the lightning strike, which will give an additional term to the vertical electric field. For an infinite current channel, the charge is separated by an infinite distance. Therefore the Φ term can be neglected if the channel is electrically neutral. Only the vector potential is needed to calculate the electric field. The electric field is therefore:

$$\begin{aligned} \vec{E} &= -\frac{\partial\vec{A}}{\partial t} \\ &= -\frac{\mu_0 I_0}{2\pi}\frac{\partial}{\partial t}\ln\left(\frac{ct+r'}{r}\right)\hat{z} \end{aligned}$$

where $r' = \sqrt{(ct)^2 - r^2}$ has been introduced for convenience.

$$\begin{aligned}
\vec{E}_z &= -\frac{\mu_0 I_0}{2\pi} \frac{c + c^2 t/r'}{ct + r'} \\
&= -\frac{\mu_0 I_0}{2\pi} \frac{c(1 + ct/r')r'}{(ct + r')r'} \\
&= -\frac{\mu_0 I_0}{2\pi} \frac{c(r' + ct)}{(ct + r')r'} \\
&= -\frac{\mu_0 I_0}{2\pi} \frac{c}{\sqrt{(ct)^2 - r^2}}
\end{aligned} \tag{3.2.8}$$

This model breaks down for the magnetic and electric fields when $t = r/c$; both fields become infinite. Because the current turns on instantly and there is an infinite $\partial I/\partial t$ term which contributes to the fields. This means that an arbitrary input current cannot be reliably modeled as a superposition of step functions. Even if I_0 is small, the fields at all distances will be infinite at $t = r/c$. To remove this problem, the input current must be modeled as a superposition of functions which have a finite derivative.

3.2.2 Model 4b: Infinite Line Current with a Ramp Input

The cause of the infinite electric and magnetic field at $t = r/c$ is not obvious looking at the vector potential (equation 3.2.6); neither equation 3.2.8 nor 3.2.7 has a direct dependence on $\partial I/\partial t$. In model 1, a $\partial I/\partial t$ term is present in the electric field (equation 3.1.3). A step current has an infinite $\partial I/\partial t$ at $t = 0$, which causes the infinite electric field. For the magnetic field, the more simplistic magnetostatic models do not depend on $\partial I/\partial t$. Model 4 has an implicit dependence on $\partial I/\partial t$ which causes 3.2.7 to be infinite at $t = r/c$.

To avoid the infinite fields at $t = r/c$, the input current can be constructed as a superposition of ramps instead of steps, that is:

$$I(\xi) \;=\; \begin{cases} 0 & \xi < 0 \\ \frac{\Delta I}{\Delta t}\xi & \xi > 0 \end{cases} \tag{3.2.9}$$

where $\Delta I/\Delta t$ is the slope of the ramp, and $\xi = t - \eth/c$ as before. It is more complicated to build an arbitrary sequence out of a number of ramp functions than it is of steps. A generic function will usually require twice as many superimposed ramps to construct as steps because each ramp must be turned off. A triangular function such as presented earlier in Figure 3.1.2a happens to be particularly easy to generate with ramps; this is not the case for an arbitrary current.

An unfortunate side effect of using superimposed ramps to simulate the input current is that a single ramp does not give useful physical insight. With a single step, the electric field drops off to zero and the magnetic field approaches the magnetostatic limit as $t \to \infty$. With a single ramp, both fields quickly diverge to infinity. However, these downsides are offset by the benefit of finite fields at $t = r/c$.

The vector potential for a ramp function when $t > r/c$ is given by

$$\begin{aligned} A_z(r,t) &= \frac{\mu_0}{2\pi}\int_0^{z_m} \frac{\Delta I(t-r/c)/\Delta t}{\sqrt{r^2+z^2}}\,dz \\ &= \frac{\mu_0 \Delta I}{2\pi}\int_0^{z_m}\left(\frac{t}{\Delta t\sqrt{r^2+z^2}} - \frac{1}{c\Delta t}\right)\,dz \\ &= \frac{\mu_0 \Delta I}{2\pi}\left(\frac{t}{\Delta t}\ln\left(\frac{ct+\sqrt{(ct)^2-r^2}}{r}\right) - \frac{\sqrt{(ct)^2-r^2}}{c\Delta t}\right) \end{aligned} \tag{3.2.10}$$

Thus the magnetic field is:

$$\begin{aligned} \vec{B} &= \nabla \times \vec{A} = \frac{\partial}{\partial r}\vec{A} \\ B_\phi &= \frac{\mu_0 \Delta I}{2\pi}\left(\frac{t}{\Delta t}\frac{ct}{rr'} + \frac{r}{c\Delta t r'}\right) \\ &= \frac{\mu_0 \Delta I}{2\pi c r \Delta t}\sqrt{(ct)^2-r^2} \end{aligned} \tag{3.2.11}$$

and the electric field is:

$$\begin{aligned} E_z &= -\frac{\partial A_z}{\partial t} \\ &= -\frac{\mu_0 \Delta I}{2\pi}\left(\frac{1}{\Delta t}\ln\left(\frac{ct+r'}{r}\right) + \frac{t}{\Delta t}\frac{c}{r'} - \frac{c^2 t}{cr'\Delta t}\right) \\ &= -\frac{\mu_0 \Delta I}{2\pi \Delta t}\left(\ln\left(\frac{ct+\sqrt{(ct)^2-r^2}}{r}\right)\right) \end{aligned} \tag{3.2.12}$$

where $r' = \sqrt{(ct)^2 - r^2}$ has again been temporarily introduced.

Figure 3.2.1 shows the results of using the current waveform from Figure 3.1.2a as the input for equations 3.2.12 and 3.2.11. The electric field waveforms 1 km away from the lightning channel show amplitudes of around -1 kV/m, which agrees with measurements. The magnetic field has an initial peak with amplitudes about a factor of 2 larger than those seen in the magnetostatic models 1-3. After the initial peak, the magnetic field quickly drops to values closer to those seen in models 1-3 with a linear falloff which has a small overshoot. Both the

electric and magnetic fields show 2 cusps: one 2 μs after the beginning of the waveform, the other 50 μs after the beginning of the waveform. These are produced because the input current has a discontinuous time derivative at these times. Far from the current channel, the amplitudes of the fields fall off slower than the expected $1/r$, as shown in Figure 3.2.2. The slower than expected falloff is a result of assuming an infinite line current. If the current line has a finite height, the range dependence becomes the expected $1/r$. This will be shown in model 5.

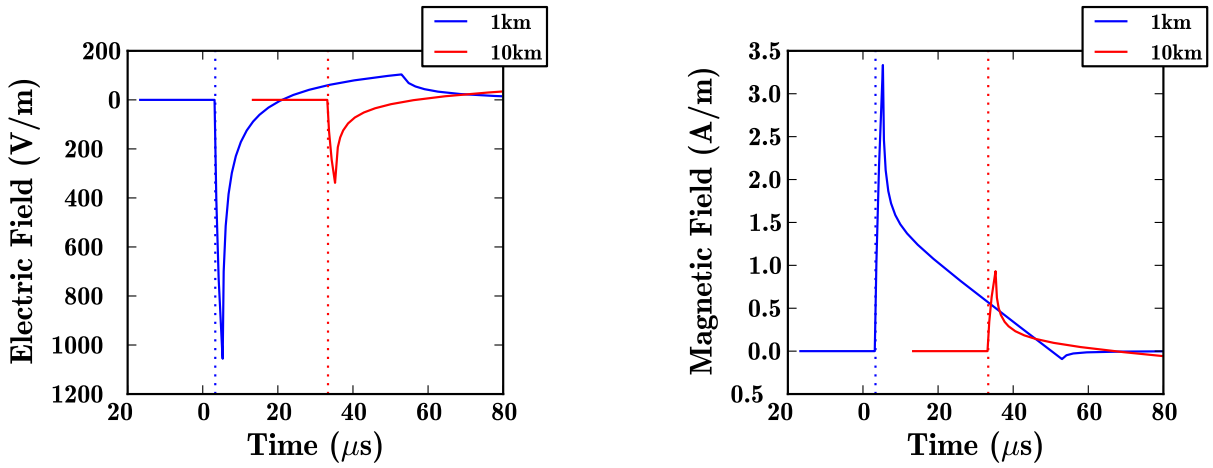

(a) Electric Field

(b) Magnetic Field

Figure 3.2.1: The electric and magnetic for model 4 constructing the current input shown in Figure 3.1.2a as a sequence of ramp functions. The dotted lines show the expected delay times $t = r/c$.

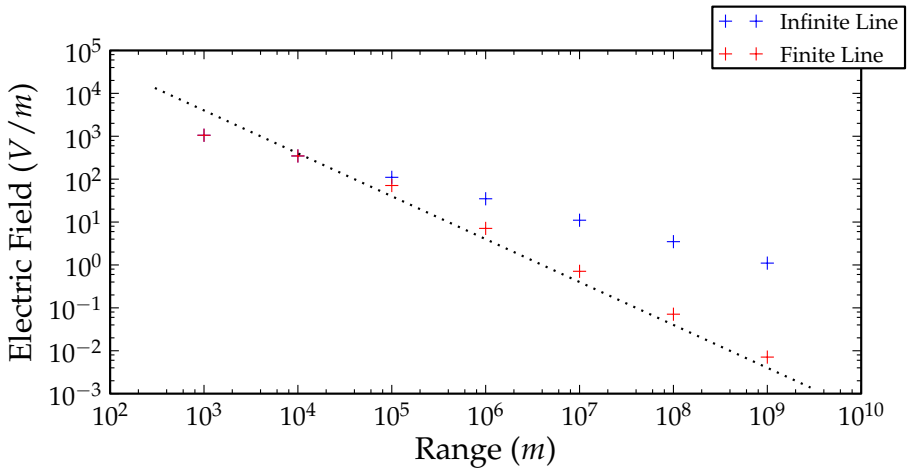

(a) Peak value of the electric field

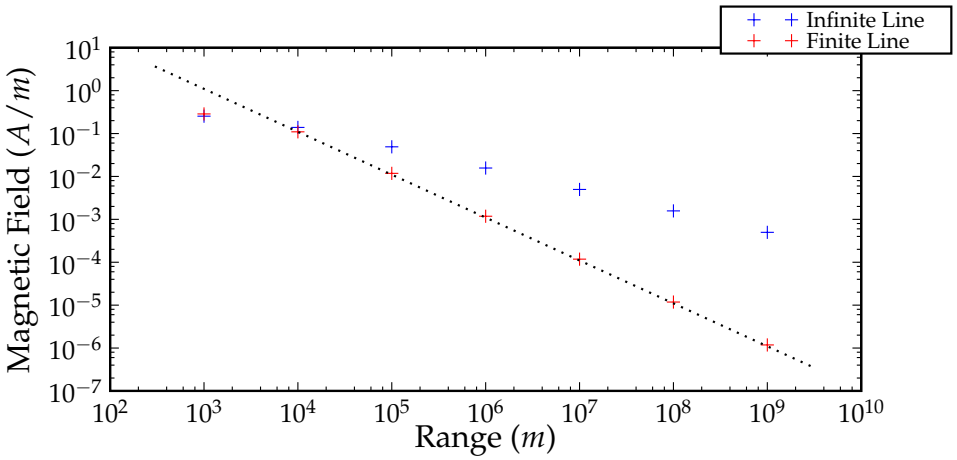

(b) Peak value of the magnetic field

Figure 3.2.2: Range dependency of the peak fields produced by model 4b (blue) and model 5 (red). The black dotted line represents the expected $1/r$ falloff.

3.2.3 Model 5: Finite Length Line Current

The next step in more accurately modeling the electric and magnetic fields of a return stroke is to have the current channel be a finite length. An infinite length current channel moves charge to a reservoir infinitely far away; this means that $\Phi = 0$. With a finite length current channel, this is no longer the case. Because $\Phi \neq 0$, the electric field has an additional electrostatic term. In the case of an infinite channel, both the electric and magnetic fields fall off more slowly than the expected $1/r$. Using a model with a finite channel length should correct this inaccuracy since far from the return stroke less of the channel is seen. Limiting the current channel to a height H does not change equation 3.2.2 for the vector potential; however there is the added condition on the limits of integration that

$$0 < z < \sqrt{(ct)^2 - r^2} < H \tag{3.2.13}$$

This will increase number of time regimes in the solution from 2 to 3 [4], causing the vector potential to become:

$$A_z = \begin{cases} 0 & ct < r \\ \frac{\mu_0 \Delta I}{2\pi} \left(\frac{t}{\Delta t} \ln \left(\frac{ct + r'}{r} \right) - \frac{r'}{c\Delta t} \right) & r < ct < R_m \\ \frac{\mu_0 \Delta I}{2\pi} \left(\frac{t}{\Delta t} \ln \left(\frac{H + R_m}{r} \right) - \frac{H}{c\Delta t} \right) & ct > R_m \end{cases} \tag{3.2.14}$$

where $R_m = \sqrt{H^2 + r^2}$ is the maximum distance to the current channel and $r' = \sqrt{(ct)^2 - r^2}$. The magnetic field is then:

$$B_\phi = \begin{cases} 0 & ct < r \\ \frac{\mu_0 \Delta I}{2\pi c \Delta t r} r' & r < ct < R_m \\ \frac{\mu_0 \Delta I}{2\pi c \Delta t r} \frac{Hct}{R_m} & ct > R_m \end{cases} \tag{3.2.15}$$

where $r' = \sqrt{(ct)^2 - r^2}$ has been left in for brevity.

[4] The two regimes were not explicitly identified in equation 3.2.2; only the non-zero regime was stated.

For the electrostatic term, a simple model is to assume that the charge carried by the current stays at the end of the channel. In this case, it is not difficult to calculate the electrostatic term directly using method of images,

$$\begin{aligned}\vec{E}_Q &= \frac{1}{4\pi\epsilon_0}\frac{Q}{\beth^2}\hat{\beth} + \frac{1}{4\pi\epsilon_0}\frac{-Q}{\beth'^2}\hat{\beth}' \\ &= -2\frac{Q}{4\pi\epsilon_0}\frac{1}{\beth^2}sin(\theta)\hat{z} \\ &= -\frac{Q}{2\pi\epsilon_0}\frac{z}{\beth^3}\hat{z}\,,\end{aligned}$$

where Q is the charge at the top of the channel and $\beth'$ is the vector from the image charge to the point P. Because all the charge is deposited at the top of the lightning channel, the above equation is evaluated at $\beth = R_m$, giving:

$$\vec{E}_Q = -\frac{Q}{2\pi\epsilon_0}\frac{H}{R_m^3}\hat{z} \tag{3.2.16}$$

The charge Q can be found by integrating the current, $Q = \int I(t_r)dt$. Since the location of the charge is not moving with time, it is especially easy to handle the time it takes its information to reach point P.

$$Q = \begin{cases} 0 & ct < R_m \\ \Delta I\frac{(t-R_m/c)^2}{2\Delta t} & ct > R_m \end{cases} \tag{3.2.17}$$

Combining the electrostatic term with the field derived from the vector potential gives:

$$E_z = \begin{cases} 0 & ct < r \\ -\frac{\mu_0\Delta I}{2\pi\Delta t}\ln\left(\frac{ct+r'}{r}\right) & r < ct < R_m \\ -\frac{\mu_0\Delta I}{2\pi\Delta t}\left(\ln\left(\frac{H+R_m}{r}\right) + \frac{H(ct-R_m)^2}{2R_m^3}\right) & ct > R_m \end{cases} \tag{3.2.18}$$

Figures 3.2.3 shows the input current and vector potential of model 5. Figure 3.2.3a shows the same triangular input current used in all previous models (Figure 3.1.2a) split into the three ramps needed to construct it. Figure 3.2.3b-d show the vector potential for each individual ramp and well as the total waveform. As one goes farther from the current line, the

vector potential becomes increasingly proportional to the input current. The vertical dotted lines show when each ramp component is first seen at point P, and when the entire current line is seen. For an infinite channel (such as in model 4), one would never see the entire current channel.

Figures 3.2.4(a,c,e) show the electric field produced by model 5 for each ramp component as well as the total field. Figures 3.2.4(b,d,f) compare the electric field of models 4 and 5. Where the vector potential did not show a noticeable difference when the entire current line was seen radiating at point P, the electric field does. Each time a ramp component is seen along the entire length of the channel, there is a sharp decrease in amplitude of the electric field. Far from current channel, this reduces the peak amplitude of the field and causes the electric field to be proportional to $\partial I/\partial t$. Figure 3.2.5 is the same as Figure 3.2.4 except it shows the magnetic field. Far from the current channel, the magnetic field is also proportional to $\partial I/\partial t$.

Because the peak magnetic and electric field of model 5 is reduced when compared to model 4, both fields fall off with $1/r$ at large distances, as seen in Figure 3.2.2. The electric field is also now non-zero as $t \rightarrow \infty$ because of the electrostatic component to the field. The electrostatic component falls off with $1/r^3$. Both the electric and magnetic fields are proportional to $\partial I/\partial t$; if the current channel is treated as a transmission line this is not the case, as will be shown in model 6.

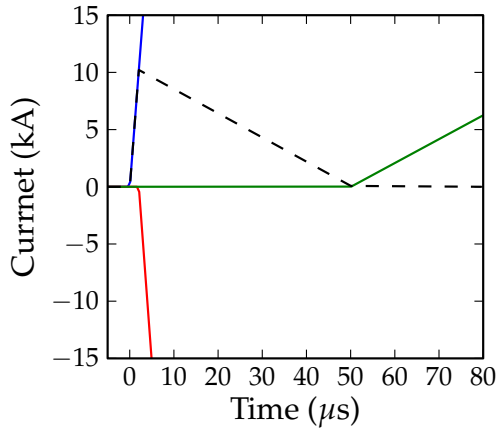

(a) Ramp components of I

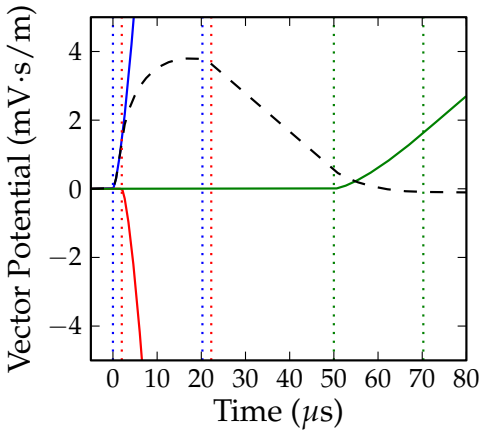

(b) Ramp Components of $\vec{A}$ at $1km$

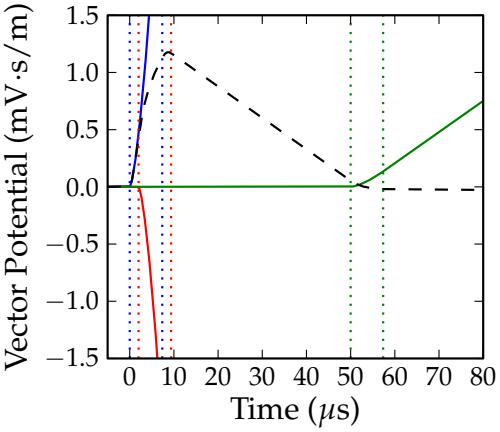

(c) Ramp Components of $\vec{A}$ at $10km$

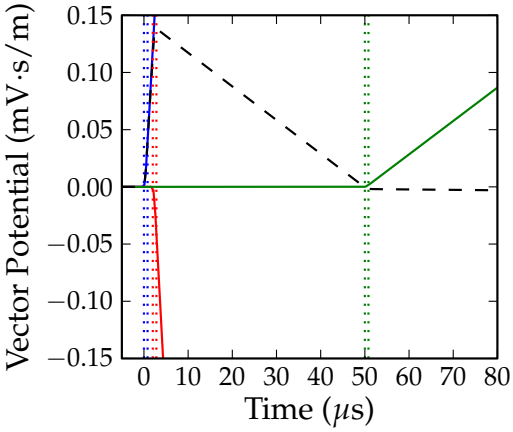

(d) Ramp Components of $\vec{A}$ at $100km$

Figure 3.2.3: (a) The input current shown as a sum of ramp functions. (b-d) The vector potential as produced by model 5 at various distances with the time delay $t = r/c$ subtracted. The vector potential for each ramp is shown individually, as well as their sum (shown by a black dashed line). The vertical dotted lines show when each ramp starts and when the entire current line is seen at point P.

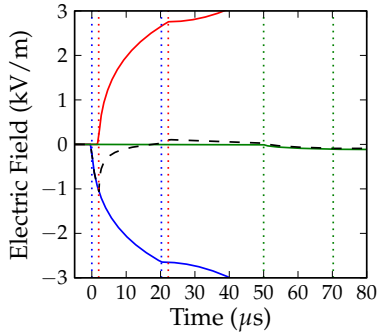

(a) Ramp Components of $\vec{E}$ at 1km

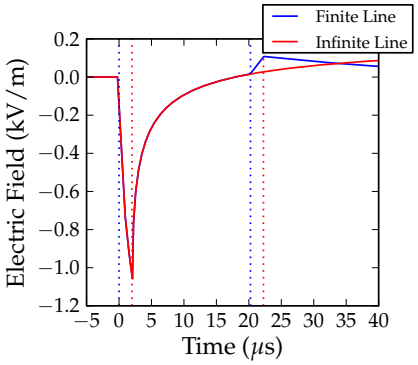

(b) Comparison with Infinite Line 1km

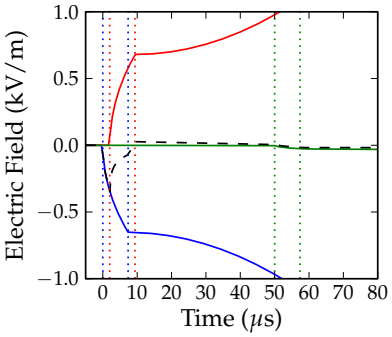

(c) Ramp Components of $\vec{E}$ at 10km

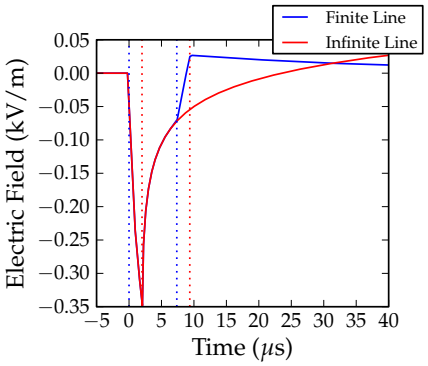

(d) Comparison with Infinite Line 10km

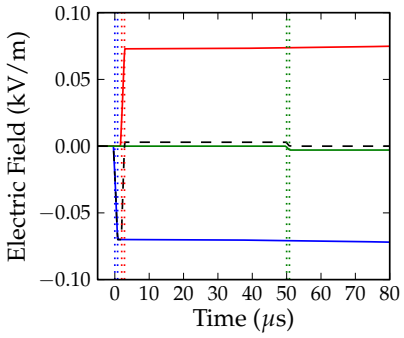

(e) Ramp Components of $\vec{E}$ at 100km

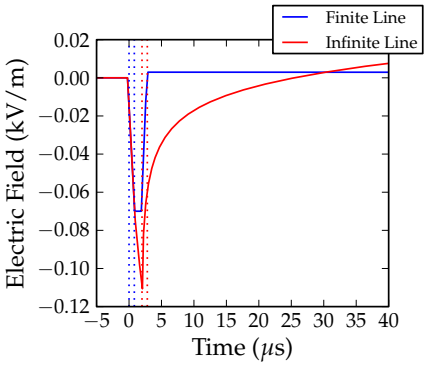

(f) Comparison with Infinite Line 100km

Figure 3.2.4: (a,c,e) Electric Field as produced by the model 5 and the current as shown in Figure 3.2.3a. The colored lines are the electric field of each component of the input current. The dashed black line is the total field. The vertical dotted lines show when each ramp starts, and when the entire current line is seen at point P. (b,d,f) Comparison of the electric field produced by model 5 with that produced by model 4b.

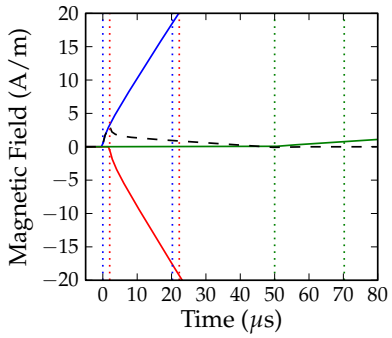

(a) Ramp Components of $\vec{B}$ at $1km$

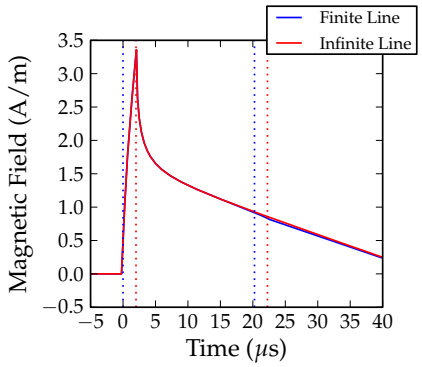

(b) Comparison with Infinite Line $1km$

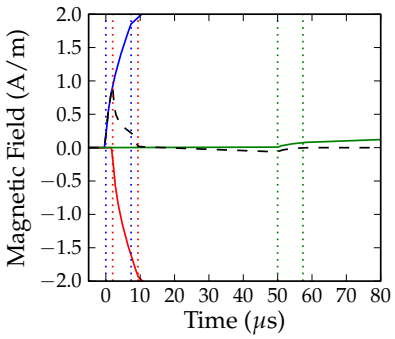

(c) Ramp Components of $\vec{B}$ at $10km$

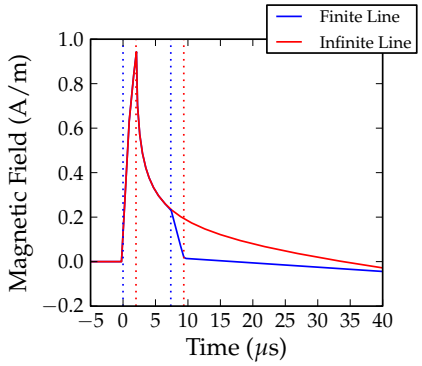

(d) Comparison with Infinite Line $10km$

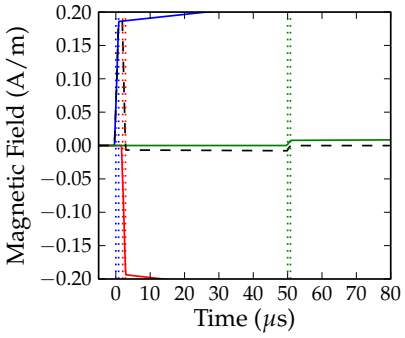

(e) Ramp Components of $\vec{B}$ at $100km$

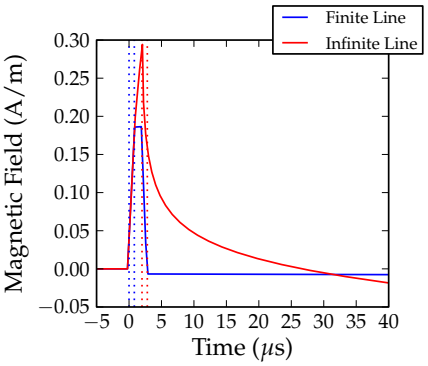

(f) Comparison with Infinite Line $100km$

Figure 3.2.5: Same as Figure 3.2.4 but for the magnetic field, B.

3.2.4 Model 6a: Transmission Line Current

In principle, it is possible to extend model 5 to allow for current to vary with position along the channel like a transmission line. However, adding in a z dependence to the current gives rise to quadratic terms in the limits which greatly complicate evaluating the integrals for the vector potential. As an alternative, the magnetic and electric fields for an arbitrary current can be obtained directly from the vector potential as first shown my Uman et al. [Uman et al., 1974] and discussed in some detail in textbooks [Uman, 1987, Rakov & Uman, 2003, Uman, 1969].

Recall that the vector potential is given by equation 3.2.2:

$$\vec{A}(r,t) = \frac{\mu_0}{4\pi}\int \frac{\vec{I}(\xi)}{\imath\!\imath} dz \tag{3.2.2}$$

The magnetic field can be found by taking the curl of equation 3.2.2, giving:

$$\vec{B}(r,t) \;=\; 2\frac{\mu_0}{4\pi}\int_0^H -\frac{\partial}{\partial r}\left(\frac{I(\xi)}{\imath\!\imath}\right)\hat{\phi}\, dz$$

The length of the return stroke is finite, so the upper limit stops at $z = H$. In addition, because the channel is over a conducting plane, the image current gives a factor or 2. Noting that $\partial\imath\!\imath/\partial r = r/\imath\!\imath$ gives:

$$\begin{aligned}
\vec{B}(r,t) &= -\frac{\mu_0}{2\pi}\int_0^H \frac{\partial}{\partial r}\left(\frac{I(\xi)}{\imath\!\imath}\right)\hat{\phi}\, dz \\
&= -\frac{\mu_0}{2\pi}\int_0^H \frac{\partial \imath\!\imath}{\partial r}\frac{\partial}{\partial \imath\!\imath}\left(\frac{I(\xi)}{\imath\!\imath}\right)\hat{\phi}\, dz \\
&= -\frac{\mu_0}{2\pi}\int_0^H \frac{r}{\imath\!\imath}\frac{\partial}{\partial \imath\!\imath}\left(\frac{I(\xi)}{\imath\!\imath}\right)\hat{\phi}\, dz
\end{aligned}$$

If the propagation delay from the current channel to the observation point P is neglected, the $\xi = t - z/v$ and the magnetic field becomes:

$$\begin{aligned}
\vec{B}(r,t) &= -\frac{\mu_0}{2\pi}\int_0^H \frac{r}{\wp}\frac{\partial}{\partial \wp}\left(\frac{I(t-z/v)}{\wp}\right)\hat{\phi}\,dz \\
&= -\frac{\mu_0}{2\pi}\int_0^H \frac{r}{\wp}\left(-\frac{I(t-z/v)}{\wp^2}\right)\hat{\phi}\,dz \\
&= \frac{\mu_0}{2\pi}\int_0^H I(t-z/v)\frac{r}{\wp^3}\hat{\phi}\,dz
\end{aligned} \tag{3.2.19}$$

This is exactly the same result seen in model 3 (equation 3.1.9). However, when the propagation delay is taking into account $\xi = t - \wp/c - z/v$. An extra term is present when taking the derivative with respect to $\wp$ because ξ is not also dependent on $\wp$:

$$\vec{B}(r,t) = -\frac{\mu_0}{2\pi}\int_0^H \frac{r}{\wp}\left(-\frac{I(t-\wp/c-z/v)}{\wp^2} + \frac{1}{\wp}\frac{\partial}{\partial \wp}I(t-\wp/c-z/v)\right)\hat{\phi}\,dz$$

The partial derivative with respect to $\wp$ can be transformed:

$$\frac{\partial}{\partial \wp}I(\xi) = \frac{\xi}{\wp}\frac{\partial}{\partial \xi}I(\xi)\,.$$

Noting that

$$\begin{aligned}
\frac{\partial}{\partial t}I(\xi) &= \frac{\partial}{\partial \xi}\frac{\xi}{t}I(\xi) \\
&= \frac{\partial}{\partial \xi}I(\xi)
\end{aligned}$$

yields:

$$\frac{\partial}{\partial \wp}I(\xi) = -\frac{1}{c}\frac{\partial}{\partial t}I(\xi)\,.$$

Using this identity, the magnetic field becomes:

$$\begin{aligned}
\vec{B}(r,t) &= -\frac{\mu_0}{2\pi}\int_0^H \frac{r}{\wp}\left(-\frac{I(t-\wp/c-z/v)}{\wp^2} - \frac{1}{\wp c}\frac{\partial}{\partial t}I(t-\wp/c-z/v)\right)\hat{\phi}\,dz \\
&= \frac{\mu_0}{2\pi}\int_0^H \left(\frac{r}{\wp^3}I(t-\wp/c-z/v) + \frac{r}{\wp^2 c}\frac{\partial}{\partial t}I(t-\wp/c-z/v)\right)\hat{\phi}\,dz
\end{aligned} \tag{3.2.20}$$

There are now two terms to the magnetic. The first term is called the inductive term, the second term is called the radiative term. At large distances, the inductive term falls off with $1/r^2$ and the radiative term with $1/r$. As has already been shown, the inductive term is due to magnetostatic processes. The radiative term is a result of the propagation delay. Models 1-3 do not include a radiation term because they do not account for a propagation delay between the current channel and the observation point P. Models 4 and 5 do include the radiation term, but it is implicit in the result.

A similar technique can be used to solve for the electric field, giving:

$$\begin{aligned} E_z &= \frac{1}{2\pi\epsilon_0}\int_0^H \left(\frac{2z^2-r^2}{\text{ת}^5}\int_0^t I(\tau-\text{ת}/c-z/v)d\tau \right. \\ &+ \left. \frac{2z^2-r^2}{c\text{ת}^4} I(t-\text{ת}/c-z/v) - \frac{r^2}{c^2\text{ת}^3}\frac{\partial I(t-\text{ת}/c-z/v)}{\partial t} \right) dz \end{aligned} \tag{3.2.21}$$

In addition to the inductive and radiative terms, the electric field has an electrostatic term which is related to the charge transfered, $\int I(t_r)dt$. The electrostatic term does not decay to zero as $t \to \infty$ and it falls off with $1/r^3$ far from the current channel.

It is possible to evaluate these integrals using a ramp current as the input, however many of the same complications encountered when solving this problem as an extension of model 5 still remain. Details of how this could be done are presented in Appendix B but have not been implemented. To produce the fields generated by model 6 taking into account the finite speed of light, the integrals were evaluated numerically. The implementation for numerical evaluation limits the input currents to triangular waveforms where the rise-time and fall-time do not have to be the same. The input current shown in Figure 3.1.2a can be described in this way.

Results of numerical integration are shown in Figure 3.2.6. The effects of treating the current channel like as a transmission line are dramatic for the electrodynamic models. In

model 6, the peak amplitudes are greatly reduced and the durations increased compared to models 4 and 5. Once the current pulse reaches the top of the channel, it suddenly disappears. This turnoff causes a sudden change in the field when the information that the pulse is at the top of the channel reaches point P, between 70 and 80 μs. The sudden change in the field strength is not physical; in a real lightning strike when the current pulse reaches the top of the channel, it distributes into the cloud in a way that is difficult to model. Because of this sudden change in field, transmission line models (models 3 and 6) can only be considered to be accurate for $t < t_0$, where t_0 is the time when the current pulse reaches the top of the channel. For a 7 km channel with a pulse traveling at 1×10^8 m/s, $t_0 = 70$ μs. Close to the channel, the sudden field change happens as much as 23 μs later because of the extra distance between the top of the channel and point P.

3.2.5 Model 6b: Simplified Transmission Line Current

It has already been shown that the inductive term of the magnetic field (equation 3.2.20) is magnetostatic in nature and was implemented in model 3 neglecting the propagation delay for any current input. Therefore the magnetic field produced by an electrodynamic transmission line can be approximated as the sum of model 3 and the radiative term of equation 3.2.20:

$$\vec{B}(t + r/c) \simeq B_{Model3}(t) + B_{rad}(t + r/c) \tag{3.2.22}$$

Shifting the magnetic field in time by r/c adds the propagation delay that model 3 does not account for. Far from the current channel $B(t + r/c) = B(t + \text{ת}/c)$, and the result is exact.

Far from the current channel $\xi \simeq t - r/c - z/v$, and the time derivative in the radiative term can be transformed:

$$\begin{aligned} \frac{\partial}{\partial z} I(\xi) &= \frac{\partial \xi}{\partial z} \frac{\partial}{\partial \xi} I(\xi) \\ &= -\frac{1}{v} \frac{\partial}{\partial t} I(\xi) \\ -v \frac{\partial}{\partial z} I(\xi) &= \frac{\partial}{\partial t} I(\xi) \end{aligned}$$

Using this identity, the radiative term of the magnetic field far from the current channel where $\eth \rightarrow r$ becomes:

$$\begin{aligned} B_{rad} &= -\frac{\mu_0}{2\pi}\int_0^H \frac{r}{c\eth^2}\frac{\partial}{\partial t}I(t-\eth/c-z/v)dz \\ &= \frac{\mu_0}{2\pi}\int_0^H \frac{v}{c\eth^2}\frac{\partial}{\partial z}I(t-\eth/c-z/v)dz \\ &= \frac{\mu_0}{2\pi r}\frac{v}{c}\int_0^H \frac{\partial}{\partial z}I(t-r/c-z/v)dz \\ &= -\frac{\mu_0}{2\pi r}\frac{v}{c}I(t-r/c)+\frac{\mu_0}{2\pi r}\frac{v}{c}I(t-r/c-t_0) \end{aligned} \tag{3.2.23}$$

where $t_0 = H/v$, the time it takes the pulse to get to the top of the return stroke. The radiative term far from the current channel can be described as two pulses separated by a time t_0 that are opposite in amplitude and proportional to the current pulse, seen in Figure 3.2.6. The radiative term has the same form as model 1 scaled by v/c.

Combining the results of model 3 with equation 3.2.23 gives an approximation of the magnetic field:

$$B_\phi(t+r/c) \sim \int_0^H \frac{\mu_0 r}{2\pi(z^2+r^2)^{3/2}}I(t-z/v)\,dz + \frac{v}{c}\frac{\mu_0 I(t)}{2\pi r} \tag{3.2.24}$$

The term involving $I(t-t_0)$ has been left out of the implementation because it has a dramatic effect on the field waveforms which is non-physical. For both the inductive and radiative terms, the approximation was made that $\eth \sim r$, so the approximation shown in equation 3.2.24 becomes more accurate the farther from the current channel point P is.

A comparison of models 6a and 6b is shown in Figure 3.2.7. The inductive term of models 6a and 6b are very similar because only the finite speed of light is not accounted for. The radiative term of model 6a and 6b show more noticeable differences. The second pulse was neglected in model 6b as previously noted. In addition, unlike the inductive term, the radiative

term of model 6b assumes $\wr = r$. As a result, the radiative term of model 6b overestimates the magnetic field close to the current channel when compared to model 6a.

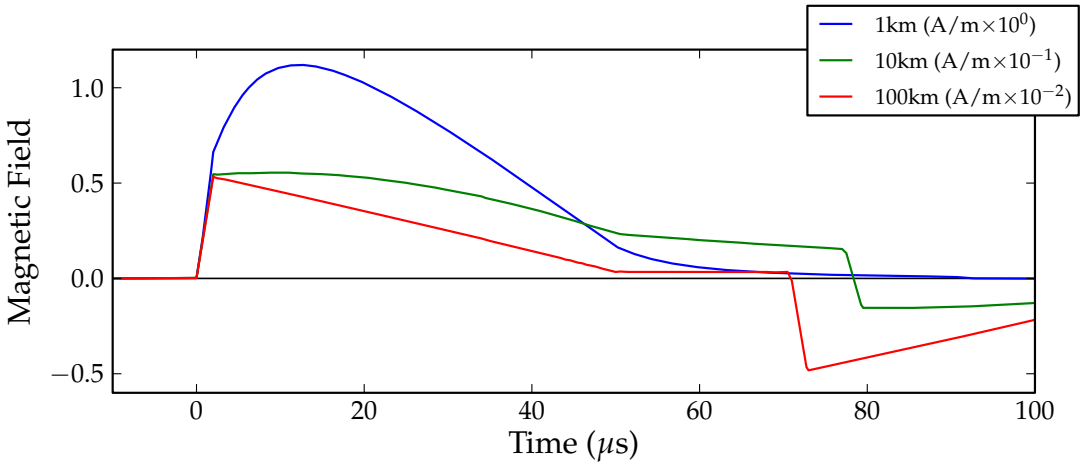

(a) Magnetic Field

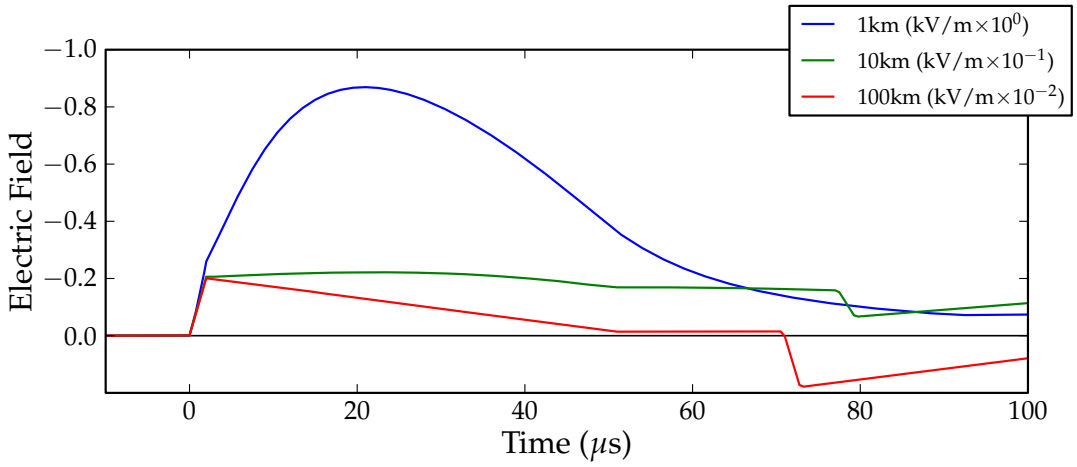

(b) Electric Field

Figure 3.2.6: Electric and magnetic fields produced by model 6a: using numerical integration of equations 3.2.21 and 3.2.20. The $1/r$ dependence in the solutions have been removed so that the waveforms at different ranges can be better compared.

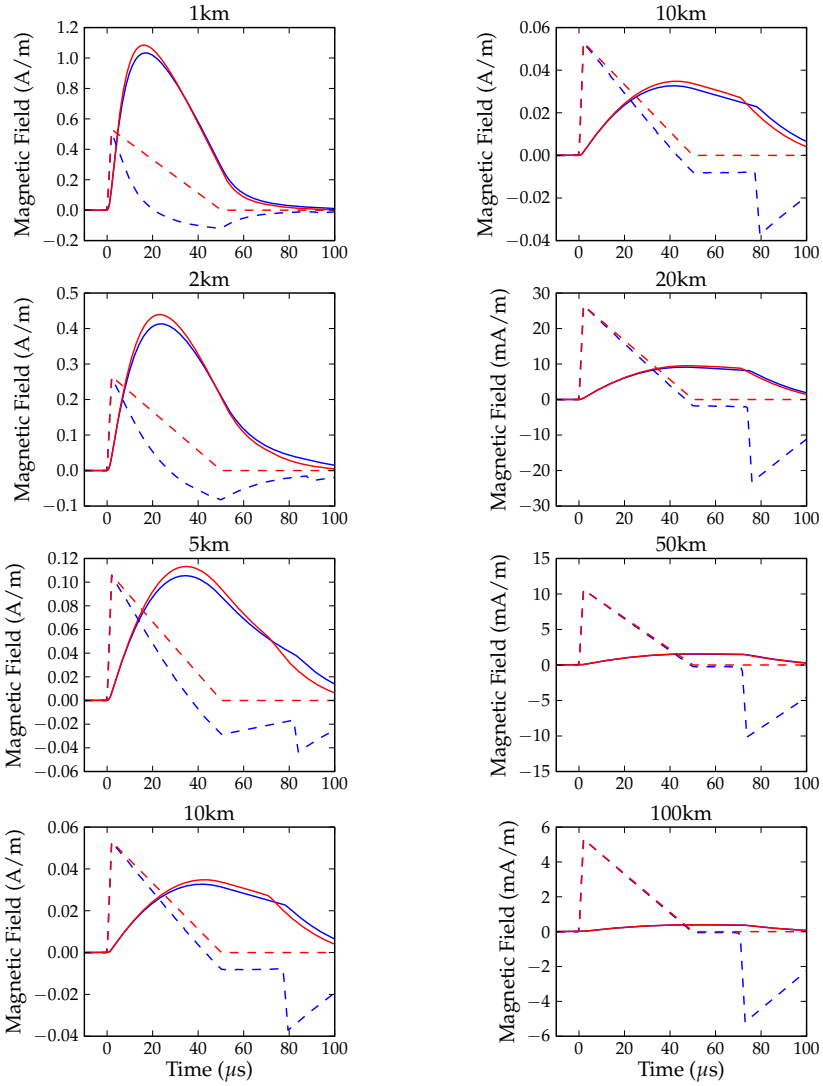

Figure 3.2.7: A comparison of model 6a (blue) and model 6b (red). Solid line shows the inductive term, dashed line shows the radiative term.

3.3 Discussion

The fields in the ground can be calculated using the diffusion equations 2.3.1 and 2.3.3 if the fields at the surface are known. While the ideal situation is to use measured fields at the surface, we can also use a model to estimate the field at the surface given the distance to the return stroke and its current. Of particular interest for this paper is the azimuthal magnetic field at the surface, since the vertical electric field is largely shielded from penetrating the ground.

In this section, six different models have been developed to estimate the fields produced by a lightning return stroke. Each model extends on the one before it, starting with magnetostatic models and moving on to electrodynamic treatments. These models culminate in a model presented by Uman which uses a current pulse traveling up a finite length transmission line to calculate the fields produced by the lightning stroke. As is always the case with models, it is possible to develop these models still farther. At this point, doing so would be of questionable value.

Evaluating how well these models work is difficult. One might expect that each model is a little bit better at approximating the field than the last. However, models 4 and 5 give vastly different fields than the rest of the models. For this discussion, we will assume that model 6b is a good representation of the true fields produced by a lightning return stroke. A comparison of a number of these models to model 6b is shown in Figures 3.3.1 and 3.3.2. In this figure, it is clear that model 5 does not produce a very good approximation of the fields produced by a lightning return stroke. The peak fields are vastly overestimated, and the duration is much too short at all ranges. The same is true of model 4 as well (not shown).

The magnetostatic models, models 1-3, match model 6b amazingly well. The peak amplitudes given by model 2 overestimate the fields close to the lightning channel, and underestimate the fields farther than about 20 km. Model 1 (not shown in Figures 3.3.1 and 3.3.2) is almost exactly a factor of 3 larger than the fields produced by model 6b far from the lightning

channel. This is because far from the lightning channel, the radiative field produced by model 6b has the same form as model 1 scaled by v/c.

The magnetic field waveform produced by model 3 exactly matches model 6b for $t > t_0$ where $t_0 = H/v$ or 70 μs. This is because model 6b calculates the inductive component of the magnetic field using model 3. For $t < t_0$, model 3 underestimates the magnetic field because it lacks the inductive component.

Comparing the models against each other does not give a good indication of how accurately the model approximates a real lightning return stroke. Surface magnetic fields are not regularly measured at Langmuir Lab, making comparing model 6 against measured data difficult. As a quick approximation, magnetic field waveforms from Uman and Rakov's textbooks [Rakov & Uman, 2003, Uman, 1969] were used instead.

The waveforms presented by Uman and Rakov have no information about if they were created by a single lightning flash, or about the current waveform that produced them. To fit model 6a to the waveforms, each waveform was digitally traced and placed on a grid. Then because the waveforms of model 6a are proportional to the current waveform at large distances, the output of model 6a was matched to the waveform for 200 km to get the parameters of the input current. Using this method, we find that a current pulse approximately 40 kA in amplitude and 50 μs in duration created the waveforms used by Uman and Rakov. A comparison of model 6 with these waveforms is shown in Figure 3.3.3. However, because it is not clear that the waveforms shown by Uman and Rakov came from the same lightning strike, this comparison should only be viewed as very approximate.

At distances closer than about 5 km, the full transmission line model heavily underestimates the peak field values; where the inductive component of the field should dominate. However, this may be partially due to fitting the model to the 200 km waveform. In addition, the duration of the modeled waveforms is significantly too short in duration. Looking at these

waveforms, it seems that modeling a return stroke as a current pulse traveling up a transmission line does not fully describe the surface field waveforms. For this study, model 6b will be used as input for the diffusion equations.

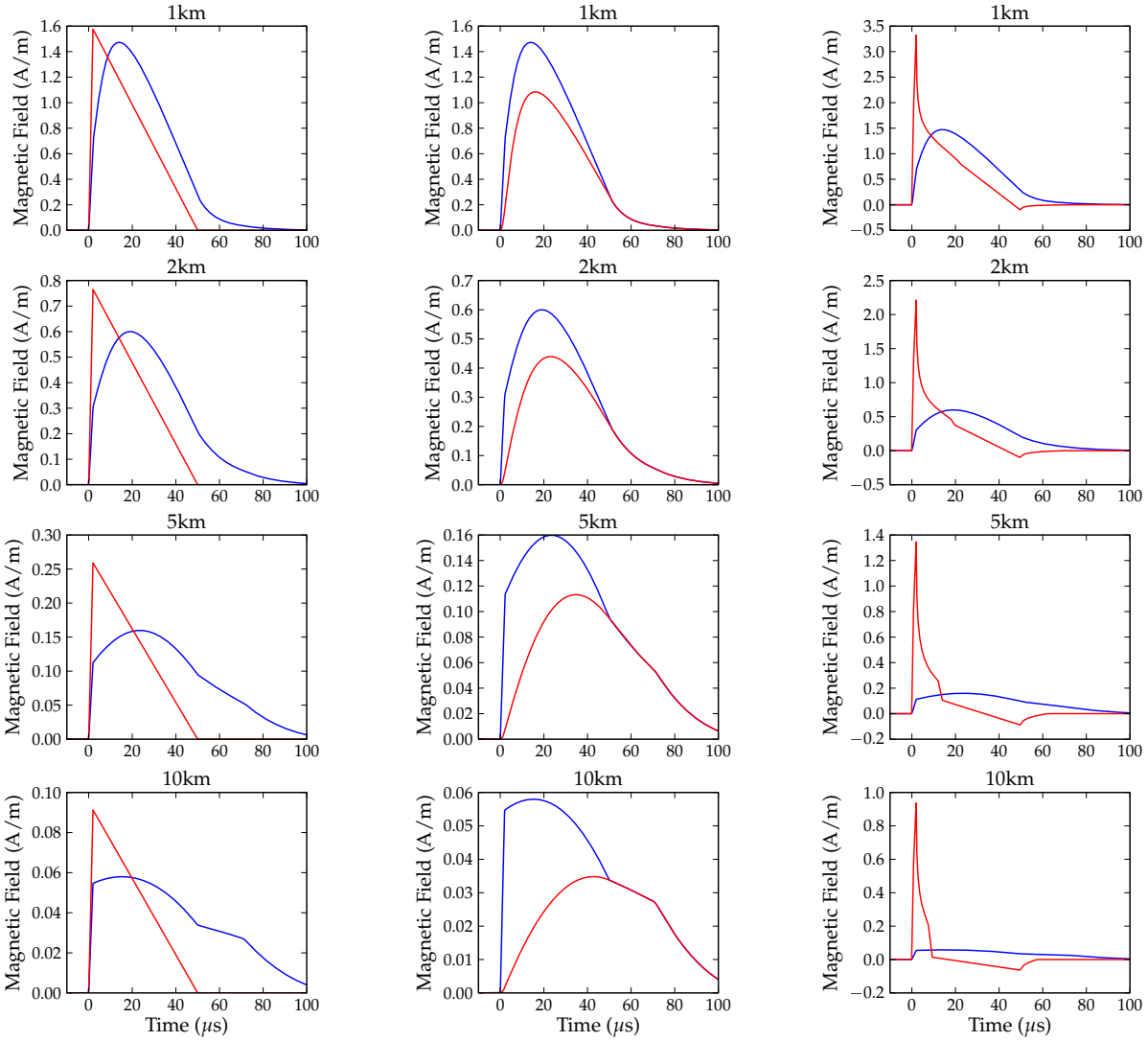

Figure 3.3.1: A comparison of different methods of calculating the magnetic field produced by a lightning return stroke for ranges from 1 to 10 km. Left compares model 6b (blue) with model 2 (red). Center compares model 6b (blue) with model 3 (red). Right compares model 6b (blue) with model 5 (red).

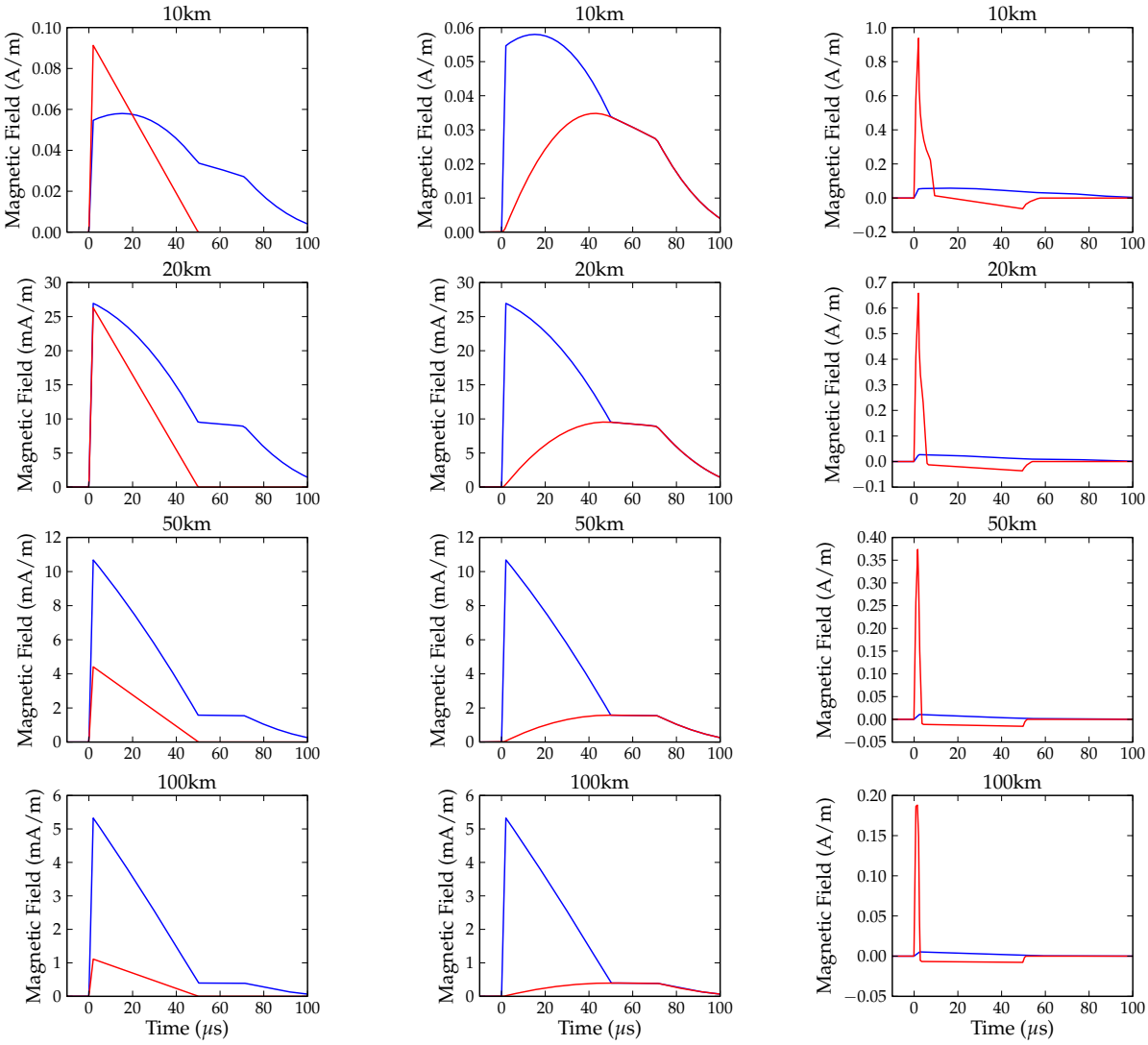

Figure 3.3.2: Same as Figure 3.3.1 but for ranges from 10 to 100 km.

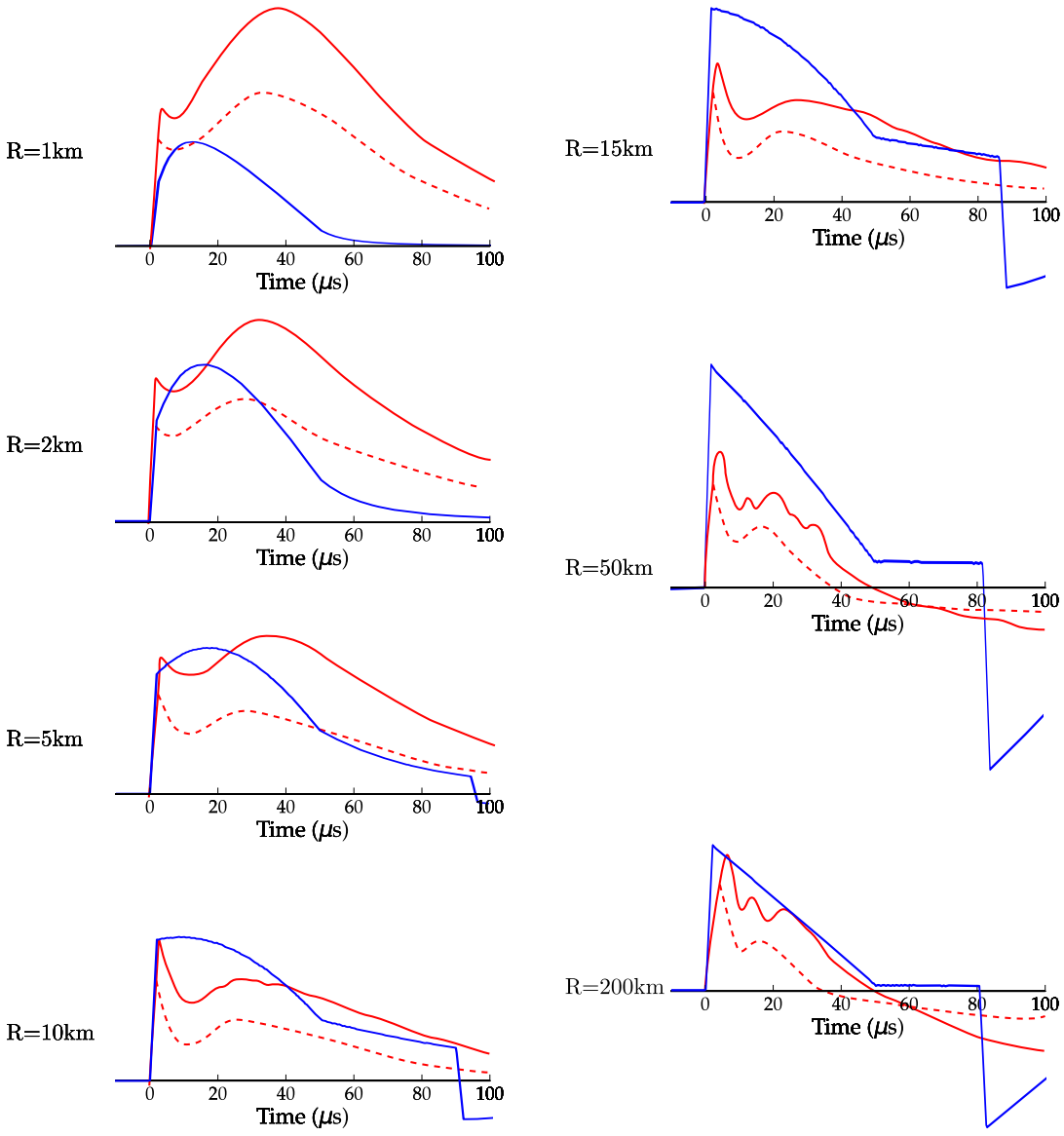

Figure 3.3.3: Results from the full transmission line model of a return stroke to fields adapted from text [Rakov & Uman, 2003, Uman, 1969]. The blue lines are results from model 6a. The red solid line is the waveform for an initial stroke, and red dashed line for subsequent stroke.

CHAPTER 4

MAGNETIC AND ELECTRIC FIELDS IN THE GROUND

All of the groundwork needed to estimate the expected fields in the Sago mine due to a lightning strike has now been completed. To calculate the magnetic field in the ground, the time-domain waveform of the surface magnetic field is converted to the frequency domain with an FFT. Then equation 2.3.1[1],

$$\tilde{B}_\phi = \tilde{B}_\phi(0)e^{(1+i)z/\delta} \tag{2.3.1}$$

is applied to get the frequency-domain waveform in the ground. The quantity $\delta = \sqrt{2/\omega\mu_0\sigma}$ is the skin depth and is frequency dependent. Finally the waveform is converted back to the time-domain with an inverse FFT. Details of this process are presented in Appendix A.

The vertical electric field is neglected; because the relaxation time of the ground is very fast, the vertical electric field does not penetrate into the ground. However, the horizontal electric field does penetrate the ground. Because the value of the horizontal electric field at the surface is not known, it is calculated from the vertical gradient of the magnetic field using equation 2.3.3:

$$\tilde{E}_r = -(1+i)\sqrt{\frac{\omega}{2\mu_0\sigma}}\tilde{B}_\phi(0)e^{(1+i)z/\delta} \tag{2.3.3}$$

The quantity $-(1+i)\sqrt{\frac{\omega}{2\mu_0\sigma}}\tilde{B}_\phi(0)$ is the horizontal electric field at the surface, $\tilde{E}_r(0)$.

As discussed at the end of Section 2.1, the same diffusion equation is a solution for B, E and J in the conductor. The $-(1+i)\sqrt{\omega/(2\mu_0\sigma)}$ prefactor in equation 2.3.3 accounts for

[1]The form of equations 2.3.1 and 2.3.3 presented here are not quite the same as those presented in Section 2.3. They have been modified to be directly applicable to this section.

Depth	50 and 100m
Resistivity	$100\ \Omega \cdot \mathrm{m}$
Length of Pump Cable	400 m
Height of Mine Shaft	2 m
Channel Length	7 km
Current Pulse Rise Time	$2\ \mu$s
Current Pulse Fall Time	$48\ \mu$s
Current Pulse Duration	$50\ \mu$s
Current Pulse Amplitude	10 kA
Current Pulse Velocity	1×10^8 m/s
Ground Conductivity[3]	∞

Table 4.1: A table of the parameters calculations in Chapter 4. Parameters for the lightning models reproduced here from Table 3.1.

converting the magnetic field boundary condition to an electric field. The z dependence of both equations 2.3.1 and 2.3.3 are the same, but the ω dependence is different.

The above solutions are presented with cylindrical coordinate labels, with $\hat{r}$ pointing away from the current channel and $\hat{\phi}$ pointing around it. This can be converted to Cartesian coordinate labels trivially by $\hat{r} \rightarrow \hat{x}$ and $\hat{\phi} \rightarrow \hat{y}$.[2] The cylindrical coordinates are used always in this section to describe the azimuth and range of the lightning strike to the sensor to avoid rotating Cartesian coordinate systems.

For all calculations in this chapter, the parameters shown in Table 4.1 are used. These parameters have been chosen because they approximate the environment of the Sago mine. The Sago mine is 100m below the surface; calculations of the electric and magnetic fields are also included 50 m below the surface to show how the waveforms change with depth.

In this chapter, plots will be shown of various waveforms diffused into the ground. In Section 4.1 the diffusion of rectangular pulses is presented to demonstrate the step and impulse

[2]This is because the solution in cylindrical coordinates can be separated to a radial and vertical part. More details on this subject can be found in Section 2.4

[3]An infinite ground conductivity is used to calculate the fields at the surface due to a lightning strike. A finite ground conductivity is then used to diffuse the fields into the ground.

response of the system. In Section 4.2 the electric and magnetic fields in the mine due to a lightning strike are estimated. In Section 4.3 the expected voltage on the pump cable is calculated, and Section 4.4 uses this to make predictions about the voltage created by the lightning strike associated with the Sago mine explosion.

4.1 Step and Impulse Responses

To investigate the step and impulse response of diffused electric and magnetic fields in the mine, unit amplitude (1 A/m)rectangular pulses are used as input to the system. Although the amplitude is not important since the fields scale linearly with the peak field at the surface, a unit amplitude pulse is especially appropriate since the magnetic field produced by a close lightning strike is on the order of 1 A/m.

Figure 4.1.1 shows diffusion acting on 1 ms, 100 μs and 10 μs rectangular pulses. The 1ms pulse is long with respect to the response time of the system, showing the step response of the system. The magnetic field at the depth of the mine increases quasi-exponentially toward the surface value after the rising edge of the pulse. After the falling edge of the pulse, there is a similar decay to zero. The 1ms B_ϕ waveform looks as though a simple low-pass filter were applied to it, however B_ϕ is smooth; at $t = 0$, both B_ϕ and $\partial B_\phi/\partial t$ are continuous. If equation 2.3.1 were acting like a simple low-pass filter $\partial B_\phi/\partial t$ would be discontinuous.

The waveform for the radial electric field is more complex. Because the prefactor of equation 2.3.3 is proportional to $\sqrt{\omega}$, the low frequencies are suppressed and the high frequency components of the waveform are enhanced. As a result, the peak radial electric field occurs earlier in the waveform, when the magnetic field at the depth of the mine is changing faster. If B_ϕ acted like a simple low-pass filter, the peak electric field would occur at $t = 0$. Because B_ϕ is initially smooth, there is a small delay between the rising edge of the pulse at the surface and the peak value of E_r in the mine. In Section 2.3, the electric field was determined

from the vertical gradient of the magnetic field, however the electric field is also proportional to $-\partial B/\partial t$. This proportionality is seen in Figure 4.1.1; where the magnetic field is increasing E_r is negative, and where the magnetic field is decreasing E_r is positive. This proportionality to $-\partial B/\partial t$ means that if a unipolar pulse of any shape and any duration is used as input to the system, the radial electric field is bipolar.

The 10 μs pulse response approximates the impulse response of the system because it is short compared to the response time of the system. The peak value of the magnetic field is greatly reduced because there is not enough time for the field to begin approaching its asymptotic value. The amplitude of the electric field is reduced less because the peak value occurs earlier. The 100 μs pulse response is intermediate between the step response and the impulse response. If a current pulse travels up a 7 km long conducting channel at 1×10^8 m/s, it will take 70 μs to reach the top. Therefore the 100 μs pulse response approximates the fields produced by a lightning return stroke.

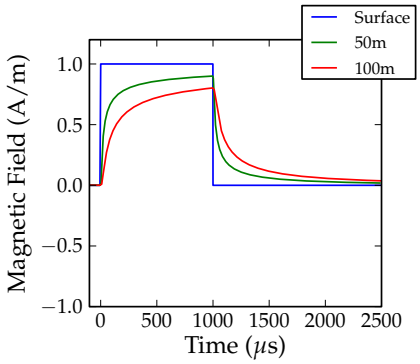

(a) 1 ms Rectangular Pulse, B_ϕ

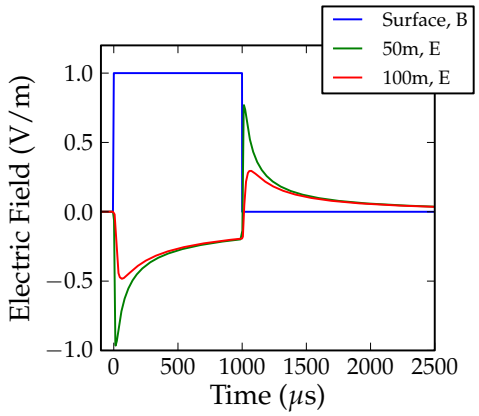

(b) 1 ms Rectangular Pulse, E_r

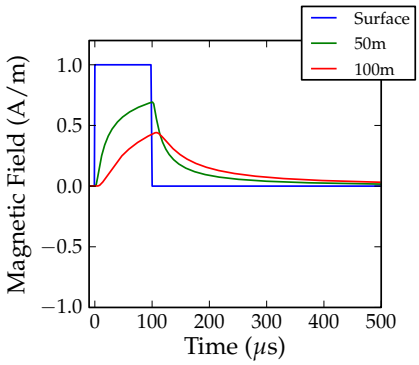

(c) 100 μs Rectangular Pulse, B_ϕ

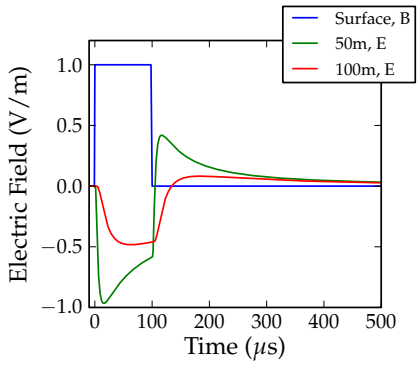

(d) 100 μs Rectangular Pulse, E_r

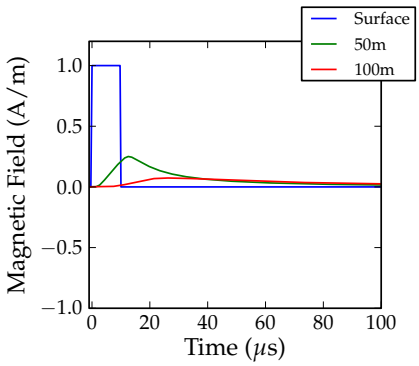

(e) 10 μs Rectangular Pulse, B_ϕ

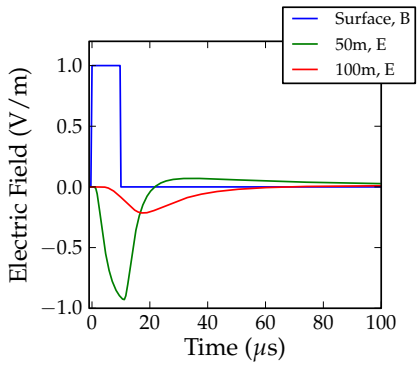

(f) 10 μs Rectangular Pulse, E_r

Figure 4.1.1: Magnetic and Electric fields in the ground produced using unit amplitude rectangular pulses as the input to the system.

4.2 Fields produced by Lightning

Equations 2.3.1 and 2.3.3 can be applied to waveforms much more complex than rectangular pulses. Of particular interest are magnetic field waveforms produced by lightning strikes. To obtain the magnetic field of a lightning strike at the surface the lightning stroke is modeled electrodynamically as a conducting line with a current pulse traveling it up like a transmission line. as described in model 6b (Section 3.2.5). The parameters for this model are listed in Table 4.1, and the surface fields can be seen in Figure 3.2.7 (pg. 57). The fields produced with model 6b for nearby strikes are shorter in duration and smaller in amplitude than those expected from a real lightning strike, as seen in Figure 3.3.3. As a result, the modeled fields in the mine may be smaller in amplitude than those actually produced by lightning. The impulsive spike seen at the beginning of the measured waveforms [Rakov & Uman, 2003, Uman, 1987] is also missing from the modeled waveforms. However, because the diffusion acts as a low-pass filter, the impulsive spike is less important than the slower hump that comes after it. In addition, a significant number of flashes should have peak currents exceeding the 10 kA used for the present calculations; the mean peak current in West Virginia is closer to 25 kA [Orville, 1990]. Amplitudes of the fields at the depth of the mine produce by using model 6b as input for the system can therefore be viewed as a lower limit what might be produced by actual lightning.

Figure 4.2.1 shows fields produced by model 6b diffused 50 and 100 m through ground with a resistivity of 100 $\Omega \cdot$ m. Model 6b is valid only for $t < t_0$, where $t_0 = 70$ μs is the time required for the current pulse to reach the top of the channel. At $t = 70$ μs, $\partial B_\phi / \partial t$ is discontinuous at the surface because the current pulse is artificially turned off when it reaches the top of the lightning channel. The modeled fields at the depth of the mine smooth this discontinuity out so that it is barely seen in the figure waveforms.

The diffused magnetic field waveforms at 100 m are about one quarter of the amplitude of the fields at the surface. The quasi-exponential tail seen in Figure 4.1.1 is still present, causing

a delayed peak field value and increasing the duration of the diffused waveforms. The horizontal electric field is several tenths of a V/m for strikes closer than about 5 km. Because the tail of the magnetic field waveform is a slow quasi-exponential decay, the positive overshoot at the end of the horizontal electric field waveform is small.

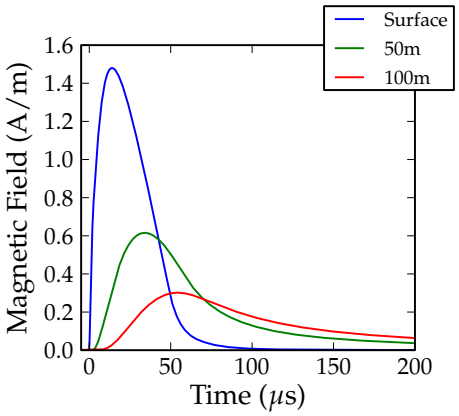

(a) 10 kA strike 1 km distant, B_ϕ

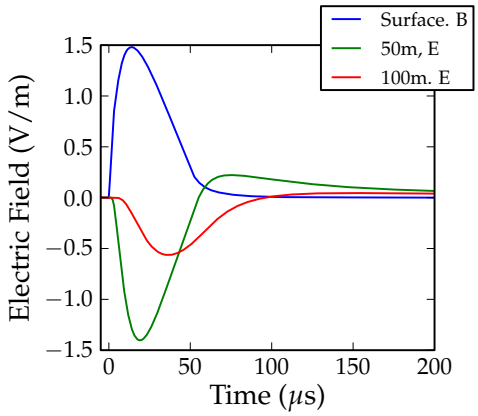

(b) 10 kA strike 1 km distant, E_r

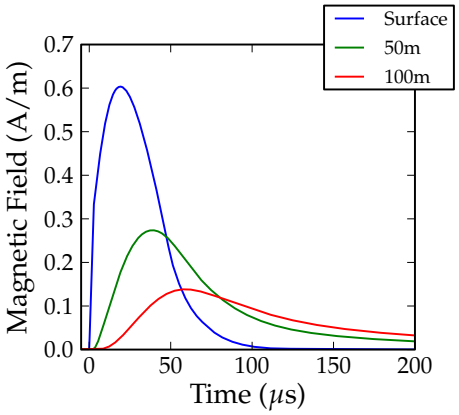

(c) 10 kA strike 2 km distant, B_ϕ

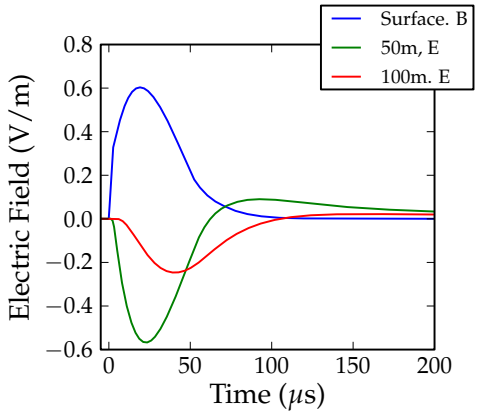

(d) 10 kA strike 2 km distant, E_r

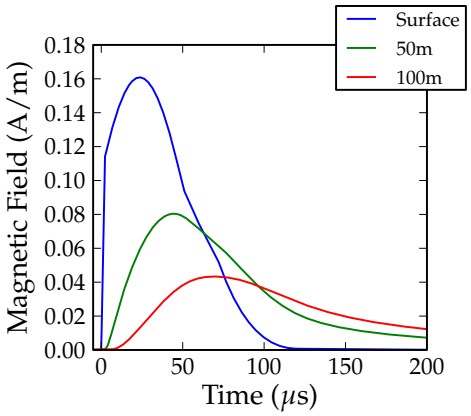

(e) 10 kA strike 5 km distant, B_ϕ

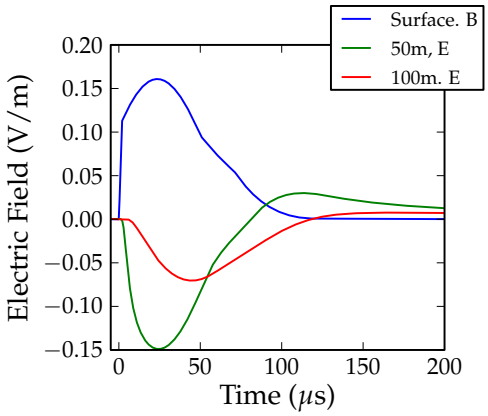

(f) 10 kA strike 5 km distant, E_r

Figure 4.2.1: Magnetic and Electric fields diffused through 50 and 100 m or 100 $\Omega \cdot$ m earth. The surface fields are produced by model 6b using the parameters shown in Table 4.1.

4.3 Estimation of Voltage in the Mine

Once the fields in the ground are known, calculating the voltage on the pump cable is straightforward. The sealed area of the Sago mine is depicted in Figure 4.3.1. It is a system of about 5 tunnels running parallel to each other 100 m below the ground, each 5 m wide, 2 m high and approximately 1000 m long. All tunnels have numerous 2 m long roof bolts on the ceiling, keeping the tunnel from caving in. Certain sections of the mine system, including the center tunnel, also have metal roof mesh bolted to the ceiling. In the center tunnel is a 400 m pump cable which is electrically connected to the roof mesh at the far end of the tunnel, and the near end lying on the floor and well insulated from the roof mesh. A sensor was connected between the pump cable and the roof mesh using the mesh as a reference to measure voltage waveforms on the cable. If a lightning strike occurs a distance D and an angle θ from the sensor, the voltage sensed by the pump cable is readily calculated from the diffused electric and magnetic fields in the ground.

There are two processes that would produce a potential difference between the end of the pump cable and the ceiling of the mine. These will be referred to as electric conduction and magnetic induction. In the case of electric conduction, the electric field in the roof of the mine causes a current to flow through the resistive medium. Because of this, there is a potential drop along the length of the mine shaft, which can be calculated as:

$$V = -\int_{L}^{0} E_r \cos(\vartheta) d\ell \tag{4.3.1}$$

where L is the length of the cable and ϑ is the angle between the pump cable and the lightning strike which is a function of position along the cable as shown in Figure 4.3.1. In addition the strength of the field is dependent on the distance d to the lightning strike, which is also a function of position along the cable. Unless the lightning strike is very close to the mine, the effect of ϑ and d being a functions of position along the cable is small, but has been included in

the calculations presented here. At large distances $\vartheta \sim \theta$ and $d \sim D$, causing the integrals to be trivial to evaluate. Equation 4.3.1 does not directly depend on the conductivity of the roof, however because the roof mesh is a good conductor the electric and magnetic fields will be attenuated an additional amount as they pass through it.

In the case of magnetic induction, the pump cable and the roof form a large open loop. The changing magnetic field due to diffusion (Figure 4.2.1) passing through this loop will induce an EMF on the open end, given by:

$$\mathcal{E} = -h \int_0^L \frac{\partial B_\phi}{\partial t} \cos(\vartheta) d\ell \tag{4.3.2}$$

where h is the height of the mine shaft.

Figure 4.3.2 shows the voltage produced on the pump cable by a modeled lightning strike at various distances to the sensor. The lightning strike was assumed to have occurred in line with the pump cable, with the pump cable between the sensor and the strike. In this way the sensed voltage is a maximum and $\cos(\vartheta) = 1$ along the entire length. The distance d doesn't show up directly in equations 4.3.2 and 4.3.1, but this will affect the amplitude of the field at the surface.

Figure 4.3.2 shows the voltage predicted by electric conduction and magnetic induction on the pump cable at a depth of 100 m. The input to the system is a simulated lightning strike modeled using model 6b (Section 3.2.5) using the parameters shown in Table 4.1. Electric conduction and magnetic induction produce a voltage with the opposite sign, however, electric conduction dominates the voltage produced on the cable. Because both electric conduction and magnetic induction methods have an approximate $\cos(\theta)$ dependency, electric conduction will dominate the voltage on the pump cable at all angles and all distances.

Table 4.2 summarizes the peak voltages seen in Figure 4.3.2. The peak total voltage is not the sum of the electric conduction voltage and the peak magnetic induction voltage because

Distance	Electric Conduction	Magnetic Induction	Total
1 km	−294 V	+14.0 V	−284 V
2 km	−114 V	+5.01 V	−111 V
5 km	−30.6 V	+1.21 V	−29.8 V
10 km	−10.7 V	+0.449 V	10.4 V

Table 4.2: A summary of the peak values seen in Figure 4.3.2.

the peaks happen at different times. Because the voltage on the pump cable is dominated by electric conduction, pump cable voltages can be estimated from Figure 4.2.1 by simply multiplying the peak electric field strength by the length of the pump cable. Close to the strike, the length of the pump cable is a significant fraction of the total distance to the strike. Since these calculations were done with the pump cable pointing towards the return stroke, making the voltages shown in Figure 4.3.2 a bit higher than one might expect looking at Figure 4.2.1.

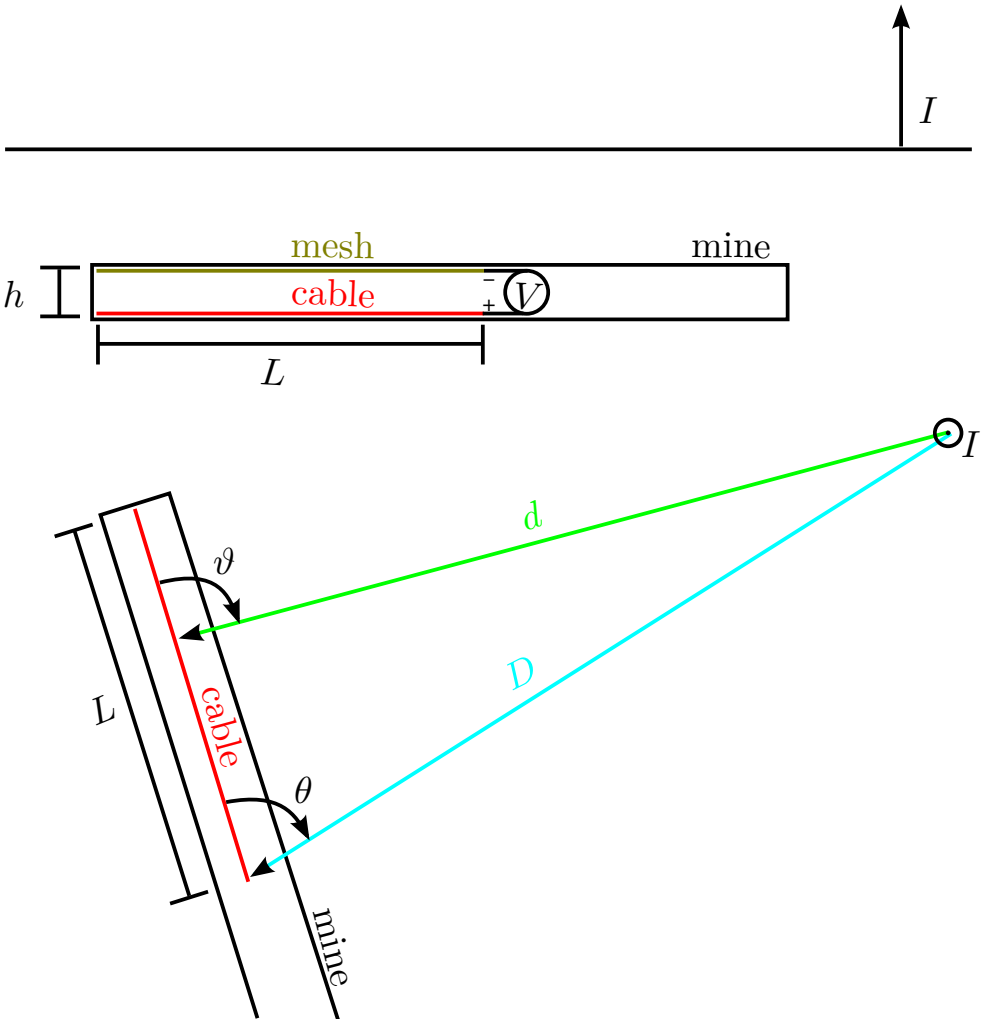

Figure 4.3.1: Sketch of the physical layout of the Sago mine.

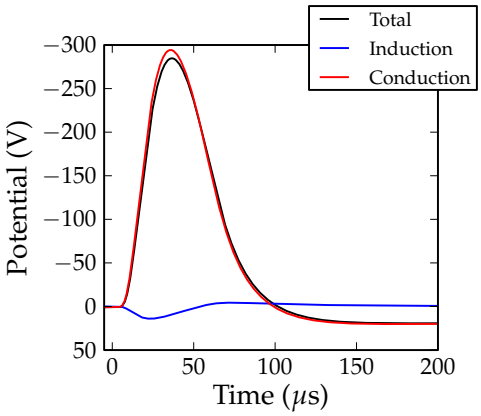

(a) 10kA strike 1km distant

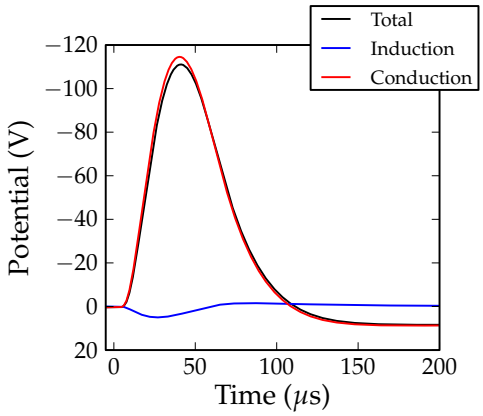

(b) 10kA strike 2km distant

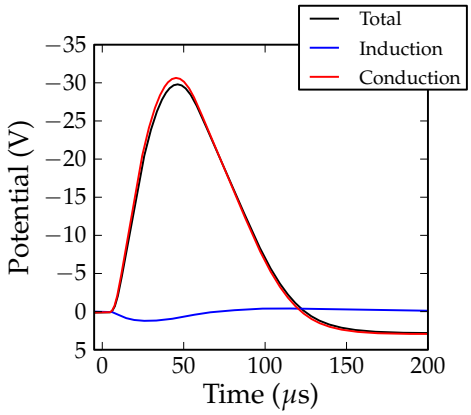

(c) 10kA strike 5km distant

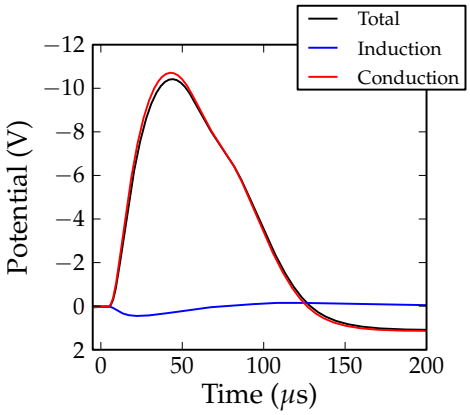

(d) 10kA strike 10km distant

Figure 4.3.2: Estimated voltage seen on the pump cable caused by magnetic induction and electric conduction. Surface fields are calculated using model 6b of a lightning strike using parameters shown in Table 4.1

4.4 Discussion

In Section 4.3 it was demonstrated if the measured potential difference between the pump cable and the roof is caused by a diffusive process, one can determine the expected amplitudes for measurements made in the mine. Electric conduction (equation 4.3.1) was found to dominate the potential difference between the pump cable and the roof. Extending this calculation to a typical lightning strike allows the prediction of the expected voltage measurements in the Sago mine.

As discussed in Section 4.2, the mean peak current for lightning flashes in West Virginia is about 25 kA [Orville, 1990]. Because the fields in the mine scale linearly with peak current, the peak voltage expected from a 25 kA strike is a factor of 2.5 larger than the peak voltage calculated for a 10 kA strike. The waveforms have an approximately $\cos(\theta)$ dependence, adding a factor of $2/\pi \sim 0.64$ to the average expected absolute peak voltage. The peak voltages shown in Figure 4.3.2 can be converted to the average expected peak voltage by simply multiplying by $2.5 \times 0.64 = 1.6$.

The range dependence is quite important. The flash density in West Virginia is fairly low, approximately 2.5 flashes/km^2/year [Orville, 1991]. There is only about a 20% chance of seeing a lightning within 0.5 km of the end of the pump cable over the course of a month. Because the area increases with D^2, the probability of seeing a flash within 2 km is quite a bit larger. Flashes within 5 km should be relatively common.

Using the values from Table 4.2, a 25 kA strikes within 5 km should be common, and are expected to produce peak voltages around 45 V. 25 kA strikes within 2 km should be uncommon, but should occur in the course of a month producing peak voltages of around 175 V. Strikes that are closer than 1 km should be rare, but if they occur they will likely produce voltages on the pump cable in excess of 300 V.

Voltages of this range are roughly consistent with the data obtained in 2008, but are significantly smaller than the voltages measured in 2007. However, there is evidence that other effects were taking in place in 2007 because the expected $\cos(\theta)$ dependence of the voltage at the pump cable was absent. In 2008 a $\cos(\theta)$ dependence was well documented.

The lightning flash thought to have caused the explosion in the Sago mine had a peak current of +101 kA and was 2 km from the location of the sensor (the epicenter of the explosion). Using the method presented above, the peak voltage on the pump cable produced by such a lightning strike should be approximately 1150 V. 1150 V is not enough to cause corona discharge, but may be large enough to cause a spark to another object if the separation is small enough.

The numbers presented above are very rough estimates, there are a number of considerations that may change the results. The surface fields produced by the transmission line model of Section 3.2.4 underestimate the amplitude and duration of the fields, especially close to the return stroke. This can be seen in Figure 3.3.3. Both a larger amplitude and longer duration of the fields at the surface will increase the fields in the mine, therefore increasing the potential difference between the pump cable and the roof.

Perhaps a bigger consideration is the roof itself. The top of the mine shaft is covered in metal roof mesh which keeps small rocks from falling on miners. This roof mesh is held in place by approximately 2 m long metal bolts which are actually what hold up the roof. This roof mesh and bolt combination cause the ceiling of the mine shaft to be a good conductor. This will cause the roof mesh to attenuate the fields diffusing into the mine. However because this layer is not very thick, the effect is small. There is also a large depth of the ground between the mine and the surface which has resistivities greater than 100 Ω·m, perhaps offsetting the shielding effect of the roof mesh. All of the considerations discussed here will be examined in more detail subsequent to the present study.

APPENDIX A

NUMERICAL IMPLEMENTATIONS

The numerical implementation of the solutions to the diffusion equations without boundary terms is fairly straight forward. The basic idea is to use an FFT to convert a time domain array for the surface field into the frequency domain. Then the transfer function shown in equation 2.3.2 is trivial to apply. Finally, invert the FFT to get back to the time domain. However, there are some details that need to be investigated to ensure the results are correct.

A.1 Discrete Fourier Transforms

For simple waveforms, the transformation to the frequency domain can be done manually. For arbitrary waveforms, Discrete Time Fourier Transform (DTFT) methods can be used. When using a DTFT special care must be taken on a number of points.

The DTFT is defined as

$$X_d(\omega) = \sum_{n=0}^{\infty} x[n]e^{-in\omega T}$$

where $x[n]$ is the input sequence of the waveform sampled at period T and $X_d(\omega)$ is defined for $-\pi/T \leq \omega < \pi/T$.[1] If the sequence $x[n]$ terminates after N elements, this becomes

$$X_d(\omega) = \sum_{n=0}^{N-1} x[n]e^{-in\omega T} \tag{A.1.1}$$

[1]Brackets are being used to denote a discrete sequence of numbers and parentheses are denote continuous functions.

The discrete sequence in time here transforms into a continuous function of frequency, which is problematic for computer simulations. To rectify this, the the output function is sampled at M evenly spaced frequencies[2] $\omega_m \in [-\pi/T, \pi/T)$ which can be described as

$$\omega_m = -\pi/T + 2m\pi/MT$$

This leads to the Discrete Fourier Transform, where both the input and the output are discrete sequences

$$\begin{aligned} X_d(\omega_m) &= \sum_{n=0}^{N-1} x[n] e^{-in\omega_m T} \\ X_d[m] &= \sum_{n=0}^{N-1} x[n] e^{-i2mn\pi/M} \end{aligned} \tag{A.1.2}$$

The final form of the DFT does not require knowledge of the sampling period T, unless the values of ω_m need to be known.

It is important to note that M is not required to be equal to N; so long as $M > N$, the inverse transform

$$x[n] = \sum_{m=0}^{M-1} X_d[m] e^{+i2mn\pi/M}$$

has no loss of information. However, most implementations of a DFT assume $M = N$, this is because if $M > N$, a new input array $y[k]$ can be defined

$$y[k] = \begin{cases} x[k], & k < N \\ 0, & N \leq k < M \end{cases} \tag{A.1.3}$$

in which case the DFT becomes

$$\begin{aligned} Y_d[m] &= \sum_{k=0}^{M-1} y[k] e^{-i2mk\pi/M} \\ &= \sum_{k=0}^{N-1} x[k] e^{-i2mk\pi/M} + \sum_{k=N}^{M-1} 0 \; e^{-i2mk\pi/M} \\ &= X_d[m] \end{aligned}$$

[2]Typically, discrete implementations define $\omega_m \in [0, 2\pi/T)$, but there can be aliasing problems for $\omega_m > \pi/T$. The frequency domain can be shifted to $\omega_m \in [-\pi/T, \pi/T)$ if this is a problem, however then negative frequencies must be dealt with.

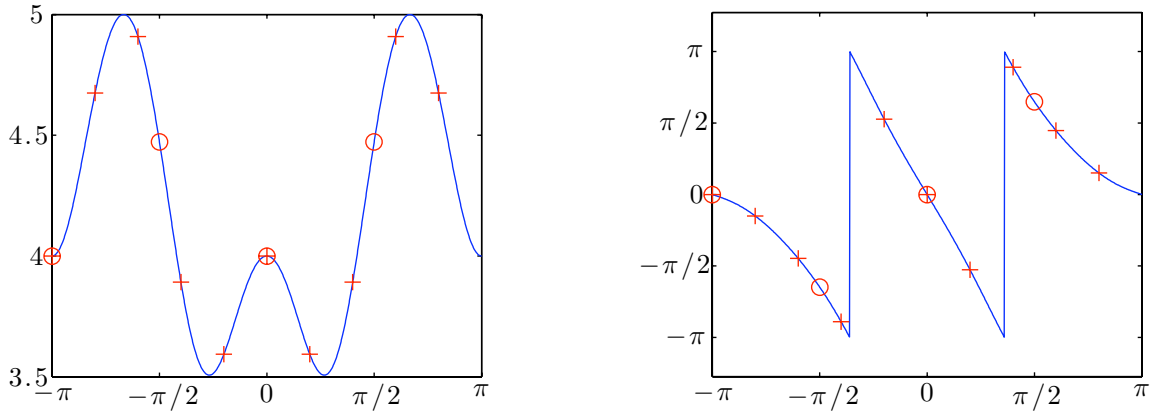

(a) Magnitude

(b) Phase

Figure A.1.1: Plot of the magnitude and phase of the DTFT of the sequence $x = [1,\ -2,\ 3,\ 2]$ (solid line) and the DFT of the same sequence with no zeros appended to the end of the sequence ($+$) and with six zeros appended to the end of the sequence ($\circ$)

This means that to increase the resolution of ω_m, all that needs be done is to pad the end of the input array with zeros.

From equation A.1.1, it can be seen that the phase of the DTFT is zero when $\omega = 0$. This is also the case with a Fourier Transform of continuous time signals. The frequency spectra of a DTFT is repeated for $\omega = 2\ell\pi/T$ for integer values of ℓ, therefore

$$\angle X_d(\omega_m = \ell\pi/T) = 0 \qquad \forall \ell \in \mathbb{N} \tag{A.1.4}$$

This is a departure of the behavior of a Fourier Transform, and can cause a distortion of the phase of some signals. Such a signal is $x(t) = e^{-at}$ for $t > 0$ where the constant $a > 0$. The transforms for this continuous time signal are

$$\begin{aligned} X(\omega) = \mathcal{F}(x(t)) &= \frac{1}{i\omega + a} \\ X_d(\omega) = \sum_{n=0}^{\infty} e^{-anT} e^{-i\omega nT} &= \frac{1}{1 - e^{-aT} e^{-i\omega T}} \end{aligned}$$

If the phase of each of these is plotted, it is quite clear that the DTFT phase is significantly different than the CTFT phase for $\omega T > \pi/5$ (see figure A.1.2). This is also not a contrived

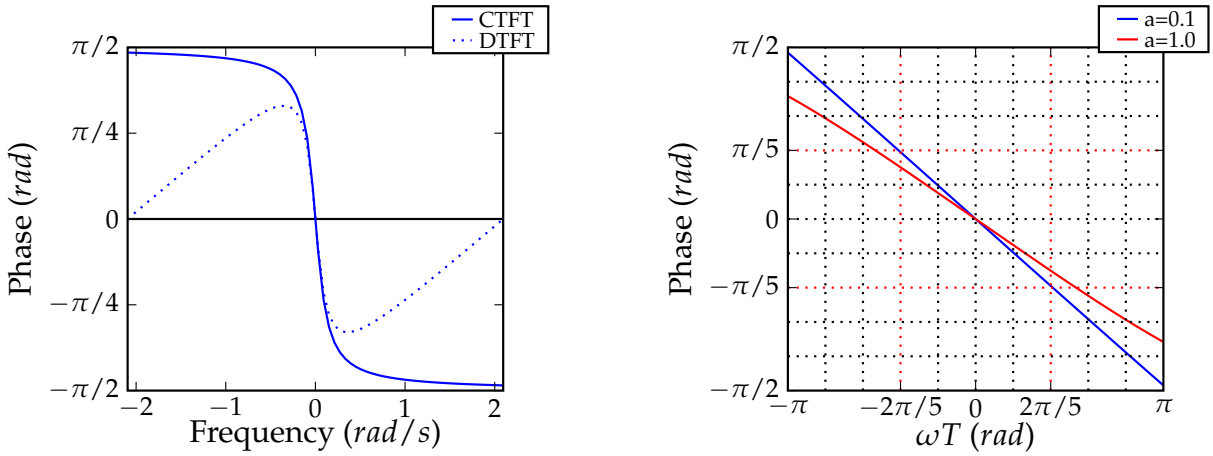

(a) Phase

(b) Phase Difference

Figure A.1.2: (a) Plot of the phase angle of the DTFT and CTFT of $x(t) = e^{-at}$ for $a = 0.1$. (b) Plot of the difference of the phase angle of the CTFT and DTFT for $a = 0.1$ and $a = 1.0$.

input; signals with exponentially decaying tails are common, especially in the input signals that might be used in this model. The solution is to over-sample the input signal by about a factor of five beyond what would be expected for the maximum frequency of interest.

A.2 Diffusion Equations in a Uniform Conductor

Once an input array in time-domain is converted to frequency domain with a DFT, applying the transfer function for the uniform diffusion equation is easy. If the input field at the surface is $f(t)$, then this is transformed into the frequency domain with $\mathcal{F}(f(t)) \rightarrow F(\omega)$. The transfer function can be applied by multiplying and can then be transformed back to the time domain, yielding

$$y(t) \;=\; \mathcal{F}^{-1}(H(\omega)\mathcal{F}(f(t)))$$

where $H(\omega)$ is the transfer function, given by

$$H(\omega) \;=\; \begin{cases} e^{(1+i)z/\delta} & \text{for} \tilde{E}_z \text{and} \tilde{B}_\phi \\ -(1+i)\sqrt{\omega/2\mu_0\sigma}e^{(1+i)z/\delta} & \text{for} \tilde{E}_x \end{cases}$$

The only remaining complication has to do with aliasing. The frequency range of the DFT output varies from $\omega = -\pi/T_s$ to $\omega = \pi/T_s$, but negative frequencies are not physical. This portion of the frequency domain cannot be forced to zero either, since that would be discarding half of the power in the spectrum. In addition, the simplistic implementation presented above produces a non-causal filter; the diffused waveform has a component that travels backward in time.

The solution to the problem can be seen in the property of Fourier transforms which states that if $f(t)$ is a real-valued function, then $|F(\omega)|$ is an even function and $\angle F(\omega)$ is an odd function. It is expected that $y(t)$ is also a real-valued function, which implies that $H(\omega)F(\omega)$ is even in magnitude and odd in angle. For this to happen, $H(\omega)$ must also have these properties.

However, $H(\omega)$ does not have these properties using standard conventions. This can be seen by rewriting the transfer functions in terms of $|\omega|$

$$\begin{aligned} H(\omega) &= e^{(1+i)z/\delta} \\ &= e^{(1+i)\sqrt{\omega\mu_0\sigma/2}z} \\ &= \begin{cases} e^{(1+i)\sqrt{|\omega|\mu_0\sigma/2}z} & \text{for} \omega > 0 \\ e^{(i-1)\sqrt{|\omega|\mu_0\sigma/2}z} & \text{for} \omega < 0 \end{cases} \end{aligned}$$

and this is not an even function in magnitude. Using $\sqrt{-1} = -i$, we obtain the following

$$H(\omega) = \begin{cases} e^{(1+i)\sqrt{|\omega|\mu_0\sigma/2}z} & \text{for} \omega > 0 \\ e^{(1-i)\sqrt{|\omega|\mu_0\sigma/2}z} & \text{for} \omega < 0 \end{cases} \tag{A.2.1}$$

which is even in magnitude and odd in angle. The same procedure works for the transfer function for $\tilde{E}_i$ giving

$$H(\omega) = \begin{cases} -(1+i)\sqrt{|\omega|/2\mu_0\sigma}e^{(1+i)z/|\delta|} & \text{for} \omega > 0 \\ -(1-i)\sqrt{|\omega|/2\mu_0\sigma}e^{(1-i)z/|\delta|} & \text{for} \omega < 0 \end{cases} \tag{A.2.2}$$

With the transfer functions modified for use with negative frequencies, it is fairly easy to apply them to an arbitrary input waveform in the time domain. Since the transfer function reduces the amplitude of the input waveform by two orders of magnitude at 50 kHz, an appropriate sampling rate is 500 kS/s. This level of oversampling should also account for errors relating to the phase approximations of the DFT.

After the transfer function has acted on the input, the output will appear to have been passed through a low pass filter. This means that if the input is impulsive, the output will noticeably longer in duration. Therefore the input array may need to be padded with 0's to increase the resolution of ω. This is shown in figure A.2.2.

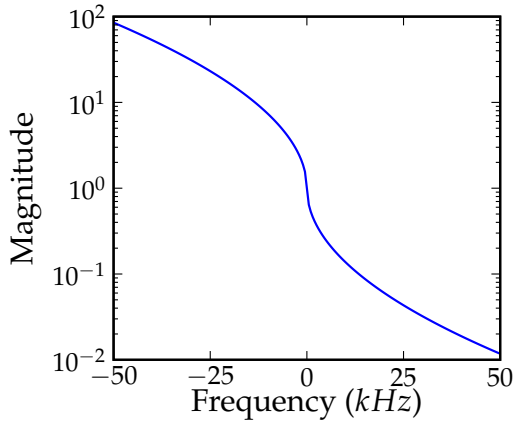

(a) Magnitude

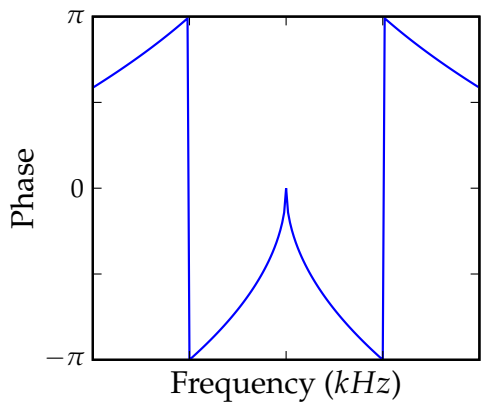

(b) Phase

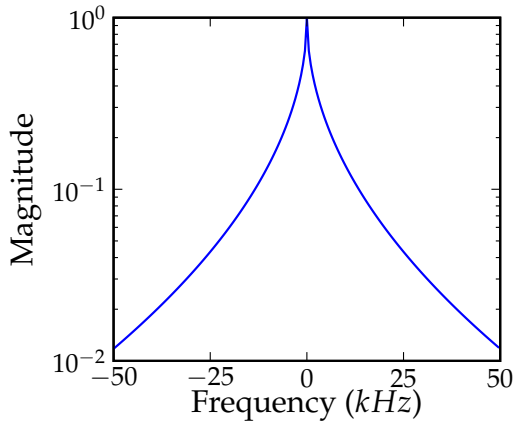

(c) Magnitude

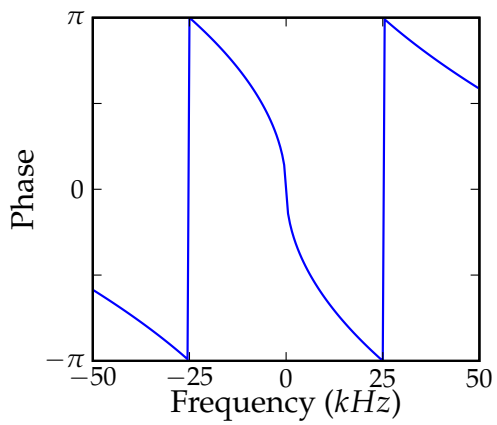

(d) Phase

Figure A.2.1: Magnitude and phase plots of the transfer function of the uniform diffusion equations for E_z and B_ϕ when choosing $\sqrt{-1} = +i$ (a,b) and $\sqrt{-1} = -i$ (c,d).

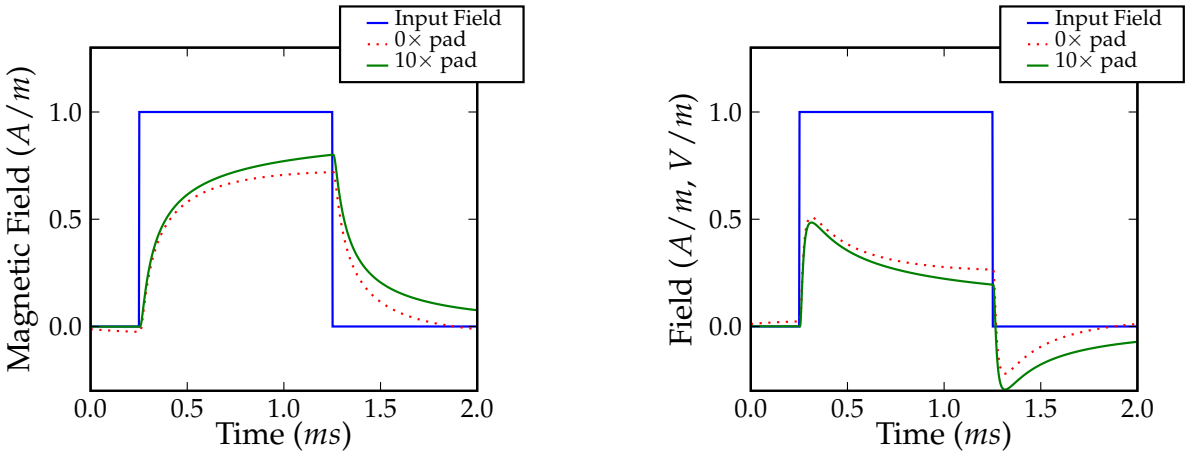

(a) Magnetic Field

(b) Electric Field

Figure A.2.2: Model results for a 1 ms long unit square pulse showing the magnetic field (a) and induced electric field (b) at $z = 100$ m. The dotted line shows the distortion of the diffused field if the resolution of the frequency array is not great enough (the input array is not padded with zeros)

APPENDIX B

ELECTRODYNAMIC TRANSMISSION LINE MODEL WITH A RAMP INPUT

Extending the same methods used to develop lightning models 4 and 5 for a transmission line input is prohibitively difficult. However solutions for the radiation produced by a finite length current channel where the current acts like a transmission line was presented by Uman et al. [Uman et al., 1974]. These solutions are:

$$E_z = \frac{1}{2\pi\epsilon_0}\int_0^H \left(\frac{2z^2 - D^2}{\wr^5}\int_0^t I(\tau - \wr/c - z/v)d\tau + \frac{2z^2 - D^2}{c\wr^4} I(t - \wr/c - z/v) - \frac{D^2}{c^2\wr^3}\frac{\partial I(t - \wr/c - z/v)}{\partial t}\right) dz \tag{3.2.21}$$

$$B_\phi = \frac{\mu_0}{2\pi}\int_0^H \left(\frac{D}{\wr^3} I(t - \wr/c - z/v) + \frac{D}{c\wr^2}\frac{\partial I(t - \wr/c - z/v)}{\partial t}\right) dz \tag{3.2.20}$$

where $\wr = \sqrt{z^2 + D^2}$. A detailed description of these equations is given is Section 3.2.4. In this section, the details for analytically evaluating the above integrals using a ramp current, $I(t) = I_0 t/\Delta t$ for $t > 0$, are discussed. As in lightning models 3-5, many ramp currents can be combined to produce an arbitrary current input. The results of the analytic treatment of the above integrals is complicated enough that numerical implementation for a ramp current was never implemented. The following is the procedure of how it might be done.

As in lightning models 4 and 5, there is height z_m which sets the upper limit of the integrals. In models 4 and 5, z_m was found by requiring $t > \beth/c$. In this transmission line treatment, the requirement becomes $t > \beth/c + z/v$, where $\beth$ is a function of z. Solving for z gives:

$$\begin{aligned} t - \beth/c - z/v &> 0 \\ (vt - z)^2 &> (\tilde{v}r)^2 \\ v^2t^2 - 2vtz + z^2 &> \tilde{v}^2z^2 + \tilde{v}^2D^2 \\ \frac{1}{\gamma^2}z^2 - 2\tilde{v}ctz + \tilde{v}^2(c^2t^2 - D^2) &> 0 \end{aligned} \tag{B.0.1}$$

where $\tilde{v} = v/c$ and $\gamma = (1 - \tilde{v}^2)^{-1/2}$ is the same term that shows up in relativity. This is a quadratic equation for z, setting it equal to zero and solving for the critical case gives

$$\begin{aligned} z &= \frac{2\tilde{v}ct \pm \sqrt{4\tilde{v}^2c^2t^2 - 4(1/\gamma^2)\tilde{v}^2(c^2t^2 - D^2)}}{2/\gamma^2} \\ &= \gamma^2\tilde{v}ct \pm \gamma^2\sqrt{\tilde{v}^2c^2t^2(1 - \frac{1}{\gamma^2}) + \tilde{v}^2\frac{D^2}{\gamma^2}} \\ &= \gamma^2\tilde{v}ct \pm \gamma\tilde{v}\sqrt{(\gamma^2 - 1)c^2t^2 - D^2} \\ &= \gamma\tilde{v}\left(\gamma ct \pm \sqrt{(\gamma^2 - 1)c^2t^2 + D^2}\right) \end{aligned} \tag{B.0.2}$$

This solution has two roots, the negative root is taken so that the integral goes to zero when $t < D/c$, as seen in figure B.0.1. Putting this all together, the maximum height, z_m, of the integral is

$$z_m = \begin{cases} 0 & t < \frac{D}{c} \\ \gamma\tilde{v}\left(\gamma ct \pm \sqrt{(\gamma^2 - 1)c^2t^2 + D^2}\right) & \frac{D}{c} < t < \frac{\Re}{c} + \frac{H}{v} \\ H & t > \frac{\Re}{c} + \frac{H}{v} \end{cases} \tag{B.0.3}$$

where $\Re = \sqrt{D^2 + H^2}$ as before.

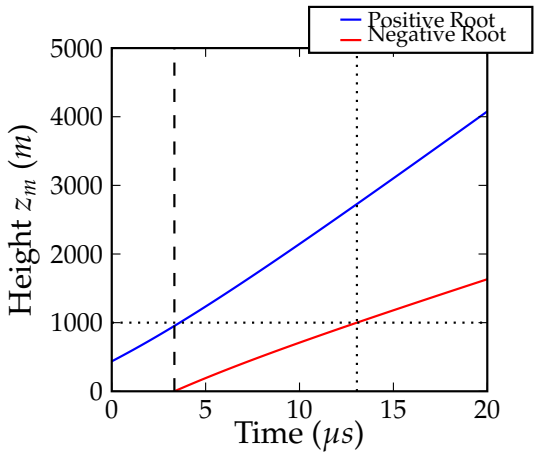

Figure B.0.1: The time dependence of the positive and negative roots for z_m, calculated at a distance $D = 1000$ m from the current channel. The vertical dashed line is $t = D/c$. The dotted lines show $t = \Re/c + H/v$ for $H = 1000$ m. This confirms that the negative root for z_m sets the upper bound for the integral.

The specific function for the current pulse can now be plugged into equations 3.2.21 and 3.2.20, starting with the time integral of the current in the electrostatic term of the electric field.

$$\begin{aligned}\int_0^t I(\tau - \frac{\eth}{c} - \frac{z}{v})d\tau &= \frac{I_0}{\Delta t}\int_{\eth/c+z/v}^{t} \tau - \frac{\eth}{c} - \frac{z}{v}d\tau \\ &= \frac{I_0}{\Delta t}\left(\frac{\tau^2}{2} - \frac{\eth\tau}{c} - \frac{z\tau}{v}\right|_{\eth/c+z/v}^{t} \\ &= \frac{I_0}{2\Delta t}\left(t - \frac{\eth}{c} - \frac{z}{v}\right)^2 \end{aligned} \tag{B.0.4}$$

Using equation B.0.4, the electrostatic term becomes

$$E_{DC} = \frac{I_0}{2\pi\epsilon_0\Delta t}\int_0^{z_m} \frac{2z^2 - D^2}{2\eth^5}\left(t - \frac{\eth}{c} - \frac{z}{v}\right)^2 dz \tag{B.0.5}$$

The inductive terms becomes

$$E_{ind} = \frac{I_0}{2\pi\epsilon_0\Delta t}\int_0^{z_m} \frac{2z^2 - D^2}{c\eth^4}\left(t - \frac{\eth}{c} - \frac{z}{v}\right) dz \tag{B.0.6}$$

And the radiative term

$$\begin{aligned} E_{rad} &= -\frac{I_0}{2\pi\epsilon_0\Delta t}\int_0^{z_m}\frac{D^2}{c^2\beta^3}\frac{\partial}{\partial t}\left(t-\frac{\beta}{c}-\frac{z}{v}\right)dz \\ &= -\frac{I_0}{2\pi\epsilon_0\Delta t}\int_0^{z_m}\frac{D^2}{c^2\beta^3}\left(1-\frac{1}{c}\frac{\partial\beta}{\partial t}-\frac{1}{v}\frac{\partial z}{\partial t}\right)dz \\ &= -\frac{I_0}{2\pi\epsilon_0\Delta t}\int_0^{z_m}\frac{D^2}{c^2\beta^3}\left(1-\frac{1}{c}\frac{zv}{\beta}-\frac{v}{v}\right)dz \\ &= \frac{I_0}{2\pi\epsilon_0\Delta t}\int_0^{z_m}\frac{zvD^2}{c^3\beta^4}dz \end{aligned} \tag{B.0.7}$$

Similar methods can be used on the magnetic field, yielding

$$B_{ind} = \frac{\mu_0 I_0}{2\pi\Delta t}\int_0^{z_m}\frac{D}{\beta^3}\left(t-\frac{\beta}{c}-\frac{z}{v}\right)dz \tag{B.0.8}$$

$$\begin{aligned} B_{rad} &= \frac{\mu_0 I_0}{2\pi\Delta t}\int_0^{z_m}\frac{D}{c\beta^2}\left(-\frac{zv}{c\beta}\right)dz \\ &= \frac{\mu_0 I_0}{2\pi\Delta t}\int_0^{z_m}\frac{-Dzv}{c^2\beta^2} \end{aligned} \tag{B.0.9}$$

These integrals can now be evaluated in closed form. However, the analytic form of the solution is complex enough to make it unwieldy to implement.

REFERENCES

[Arfken, 1985] Arfken, G. (1985). *Mathematical Methods for Physicists*. New York, NY: Academic Press, third edition.

[Dejnakarintra & Park, 1974] Dejnakarintra, M. & Park, C. G. (1974). Lightning-induced electric fields in the ionosphere. *Journal of Geophysical Research*, 79(13).

[Delfino & Rachid, 2007] Delfino, F. & Rachid, F. (2007). An algorithm for the exact evaluation of the underground lightning electromagnetic fields. *IEEE Transactions on Electromagnetic Compatibility*, 49(2).

[Golde, 1977] Golde, Ed. (1977). *Lightning*, chapter 20. Academic Press: New York.

[Griffiths, 1989] Griffiths, D. (1989). *Introduction to Electrodynamics*. Upper Saddle River, NJ: Prentice Hall, second edition.

[Higgins & Morris, 2006] Higgins, M. & Morris, M. (2006). *Measurement and Modeling of Transfer Functions for Lightning Coupling into the Sago Mine*. Technical report, MSHA.

[Jackson, 1999] Jackson, J. D. (1999). *Classical Electrodynamics*. NJ: Wiley, third edition.

[Krehbiel et al., 1979] Krehbiel, P., Brook, M., & McCrory, R. (1979). An analysis of the charge structure of lightning discharges to ground. *J. Geophys. Rsch.*, 84(C5).

[Orville, 1990] Orville, R. (1990). Peak-current variations of lightning return strokes as a function of latitude. *Nature*, 343(6254).

[Orville, 1991] Orville, R. (1991). Lightning ground flash density in the contiguous united-states - 1989. *Monthly Weather Review*, 119(2).

[Park & Dejnakarintra, 1973] Park, C. G. & Dejnakarintra, M. (1973). Penetration of thundercloud electric fields into the ionosphere and magnetosphere. *Journal of Geophysical Research*, 78(28).

[Rakov & Uman, 2003] Rakov, V. & Uman, M. (2003). *Lightning, Physics and Effects*. Cambridge, UK: Cambridge University Press.

[Sommerfeld, 1949] Sommerfeld, A. (1949). *Partial Differential Equations in Physics*. New York: Academic Press.

[Thomas et al., 2004] Thomas, R., Krehbiel, P., Rison, W., Hunyady, S., Winn, W., Hamlin, T., & Harlin, J. (2004). Accuracy of the lightning mapping array. *J. Geophys. Rsch.*, 109, D14207.

[Uman, 1969] Uman, M. (1984 (Enlarged reprint 1969)). *Lightning*. Mineola, NY: Dover.

[Uman, 1987] Uman, M. (2001 (Corrected reprint 1987)). *The Lightning Discharge*. Mineola, NY: Dover.

[Uman et al., 1974] Uman, M., McLain, D. K., & Krider, E. P. (1974). The electromagnetic radiation from a finite antenna. *American Journal of Physics*, 43(33).

[Wooten, 2006] Wooten, R. (2006). *Report of Investigation into the Sago Mine Explosion*. Technical report, West Virginia Office of Miner's Health, Safety and Training.